A Study into the Feasibility of a Human Mission to the Jovian System

Benjamin T. R. Torn
200866010

Lead Supervisor:
Dr. Matt Darnley

Supervisors:
Dr. Steve Barrett and Prof. Rolf-Dietmar Herzberg

The University of Liverpool, Department of Physics

Liverpool John Moores University, Department of Astrophysics

April 2016

Abstract

This study explores the feasibility, using current and near future technology, of a human mission to the Jovian system and the accessibility for first year undergraduates to conduct their own research and produce a viable mission plan during an ice-breaker project "Mission to the Jovian System". The study explores the possible methods of landing on one of celestial bodies within the Jovian system, protecting crew and electronics from hazardous radiation throughout the duration of the mission and safely returning the spacecraft and crew to Low Earth Orbit (LEO). The study further explores the methods of landing on a body with relatively low gravity and compiles the findings into a mission plan. Finally, the study concludes whether a mission to the Jovian system is possible with current technology and the advancements required to make such a mission accessible.

Acknowledgments

I would like to express my sincerest gratitude to my lead supervisor, Dr. Matt Darnley, for his continued support and patience throughout the project. The understanding and knowledge gained through numerous discussions during the year has considerably improved my undergraduate experience. Without the detailed feedback, this project would not be completed to the standard presented. I could not have asked for a more suitable or more friendly supervisor.

Furthermore, I would like to thank Dr. Steve Barrett and Prof. Rolf-Dietmar Herzberg for their contributions to the discussions, in areas where I previously lacked depth of knowledge.

Contents

1 Introduction

Human, interplanetary space travel is the next step in the exploration of the solar system. Since the final Apollo mission in 1972, no human has walked on another celestial body. Current missions are exploring the possibility of extending our species' reach beyond Earth's sphere of influence for the first time. National Aeronautics and Space Administration's (NASA) Orion mission is one such mission and is planning to take astronauts to Low Earth Orbit (LEO) and Mars. As a result, literature regarding manned missions to Mars is becoming more readily available for anyone with an interest, including first year undergraduates participating in the Mission to Mars project. I aim to expand the horizons of interplanetary space travel by exploring the feasibility of a human mission to the Jovian system using current and near-future technologies. This expansion of accessibility will act as a pathfinder towards evolving the Mission to Mars project.

1.1 The Jovian System

The Jovian System's main body is Jupiter, the largest celestial body in the Solar system, behind the Sun, with a radius of 71398 km at the equator, STONE and LANE (1979). As a result of its mass, it has a large sphere of influence and has many other celestial bodies orbiting within its gravitational field, giving rise to its 67 known moons; these are listed in Table 13, appendix A.1. The Jovian moons can be characterized by the types of orbits they hold: regular or irregular. There are eight Jovian moons in regular, prograde orbits: Metis, Adrastea, Amalthea and Thebe, which make up the Amalthea group, along with the four Galilean moons. The Amalthea group and the inner two Galilean moons can be seen in figure 1, the main ring of Jupiter is also highlighted. The remaining 59 known moons are all in irregular, prograde or retrograde orbits at radii larger than Callisto's (the furthest Galilean moon).

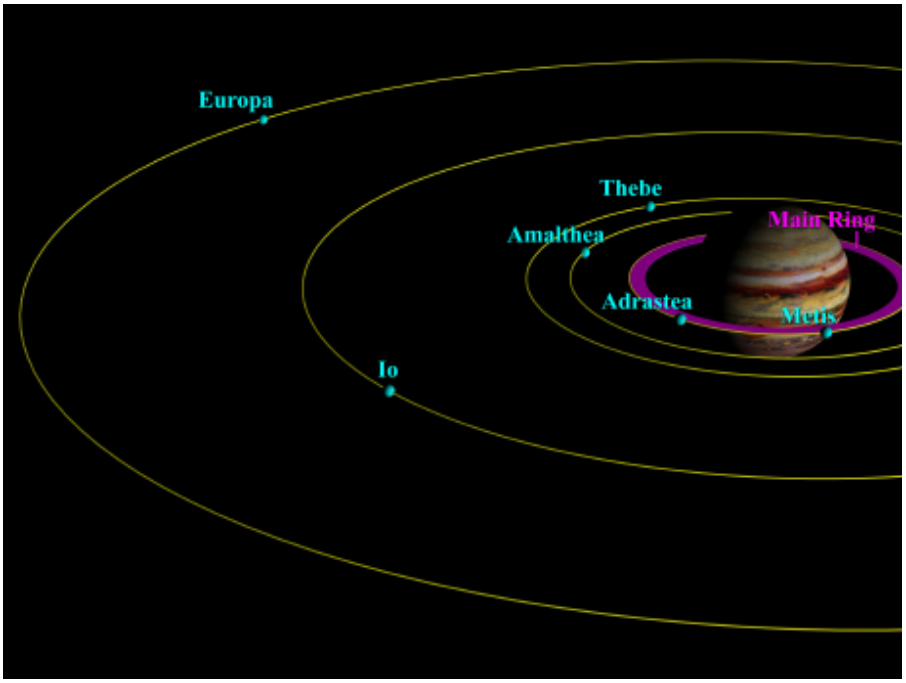

Figure 1: This Figure shows the inner satellites of Jupiter up to Europa. Ganymede and Callisto are at much larger radii and are not included, courtesy of Brand (1998).

Of the 67 known moons, the four with the largest radii are known as the Galilean moons: Io, Europa, Ganymede and Callisto, discovered by Galileo in 1610, Galileo (1610). These have the next largest radii in the solar system, behind the planets. The largest, Ganymede, has a mean

radius of 2634.1 ± 0.3 km, Showman and Malhotra (1999) ; comparable to that of Mercury's, a planet in its own right. Ganymede is the 7th moon from Jupiter, the third of the Galilean moons. The next largest Galilean moon is Callisto, the farthest from Jupiter. It has a mean radius of 2410 km and is almost twice as far from Jupiter as Ganymede. The next largest is the closest to Jupiter, Io. Io has a radius of 1880 km and is known for having extreme geological activity and being extremely volatile. Finally, Europa, the smallest of the Galilean moons, with a mean radius of only 1560 km.

1.2 Target Feasibility

In this section I endeavour to analyse the most suitable destination target, evaluating the advantages and disadvantages of each candidate in order to conclude which are feasible targets and which attributes the largest scientific interest. At the end of this section I will select a celestial body that will become the destination target for the proposed mission.

1.2.1 Jupiter

Jupiter as the fifth celestial body from the Sun is known for its giant, gaseous atmosphere, which consists of $86.4 \pm 0.3\%$ Hydrogen and $13.6 \pm 0.3\%$ Helium, Lodders and Fegley (1998), and its characteristic red spot. Possessing only a relatively small, dense core of heavier elements, it still maintains its position as the second most massive celestial object in the solar system, with a mass of $1.8986 \cdot 10^{27}$ kg, STONE and LANE (1979).

As a possible target for a human mission, Jupiter offers interesting science involving its extreme weather system and its ability to radiate large amounts of Ultraviolet (UV) rays. It also allows for an in situ study of the limits between Brown Dwarfs and gas giants to be furthered as the limits of deuterium burning can be explored. However, as Jupiter is a gas giant, a human mission would not be able to land on the surface and would have to remain in orbit, continuously being bombarded by its radiation. Studies of Jupiter are able to be conducted from orbit of one of its moons at safer distances.

1.2.2 The Amalthea Group

The largest moon in the Amalthea group is Amalthea, which has a mean radius of 83.5 km, Thomas et al. (1998). This collection of moons offer an interesting insight into the material that contributed to the formation of the solar system. However, much of the material on these moons has been contaminated by the large amounts of ionizing material erupting from Io. One interesting effect of this on the moons is that the albedo of at least three of the moons has been confirmed to be larger on the leading hemisphere than the trailing, Simonelli et al. (2000).

Due to the small size of these moons, however, the feasibility of landing a manned crew with the capabilities to survive for the 197 days required, as derived in section 3.1, poses significant problems. The low gravity ($\approx$0.002g on Amalthea) of the moons means that the escape velocities are very low ($\approx$0.05 km/s from Amalthea). As a result, equipment will not remain on the surface of the moons without being tethered at all times. Therefore, the Amalthea group is not a feasible destination.

1.2.3 Io

Io is the closest of the Galilean moons to Jupiter. It is one of the most geologically active celestial bodies, constantly ejecting sulphur and sulphur dioxide from its volcanoes into a donut-shaped ring (torus) around Jupiter, as well as giving Io its characteristic yellow colour. The cause of Io's geological activity is through the large gravitational tides exerted on it by Jupiter and the other Galilean moons. As Io orbits Jupiter the gravity it feels varies depending on where it is in its orbit. Io's orbit is pulled into a slightly elliptical orbit, being enough to disrupt its synchronous rotation around Jupiter such that the tidal forces act against its rotation. The fluctuation in

forces created by tides generates friction within the core as material is pulled in varying directions. Large portions of the material heats up creating a soft, molten core, leading to geyser like eruptions at the surface.

The crust of Io undergoes recycling at a rate of ≈1 cm per year through lava and plumes generated during volcanic activity, Schenk and Bulmer (1998). As a consequence, the majority of the surface is covered in featureless, flat planes, interspersed with geologically active mountains. There are many hypotheses as to the formation of the mountains upon Io. Plate tectonic processes responsible for the formation of mountains on Earth are not applicable as the observed mountains are found to be, for the majority, randomly distributed across the surface Kirchoff and McKinnon (2009). Neither are the mountains a formation of volcanic activity or impact craters, as on the moon. Schenk and Bulmer (1998) propose that as the new volcanic deposits are formed on the surface they force older layers to subside, increasing their density as they sink further into the moon and therefore increasing the pressure on the layer itself and other subsequent layers. The accepted method of mountain formation on Io is caused by stresses in the crust, induced by sinking layers that are relieved by thrust faulting at weaknesses, spread randomly across Io's surface.

The uncertainties surrounding the geological activity upon Io generate a large array of potential for scientific research. When considering a human mission, Io is a poor choice as a potential target due the extreme climate. Additionally, the radiation dosage on the surface of Io, partly due to its vicinity to Jupiter and partly due to the ionizing torus it generates, is such that a lethal dose would be reached if exposed for just a few minutes. Sadly, no spacesuits, as of yet, are capable of withstanding such large doses making any crew members on the surface redundant, forcing them to reside within thick layers of radiation shielding for the duration of the mission.

1.2.4 Europa

Europa's surface is entirely covered by a thick layer of water ice, up to 150 km thick, Carr Et. Al. (1997), due to its low mean surface temperature of 102K, Spencer et al. (1999), with a rocky inner core. Carr Et. Al. (1997) find evidence that suggests that large parts of the subsurface ice is in fact liquid water. This evidence is in the form of mobile 'icebergs', which are large portions of the icy crust that are moving across the surface as an iceberg would, generating the lineae on the moon's surface. This evidence of subsurface oceans align with the evidence for tidal stress within the core of the planet, similar to that of Io, due to the resonance of orbits with Io and Ganymede. The tidal effects are outlined by, Greenberg et al. (1998) and further explain the origins of the geographical features of Europa.

A subsurface ocean on Europa gives a unique opportunity within the solar system to study the implications of water on another celestial body. Within the lineae on the surface, it is thought that liquid water may flow over the current surface in a recycling process. If this is the case, landing on Europa would provide the chance of determining whether life forms could exist on other celestial body, with the potential to find life forms on Europa.

Additionally, Europa offers a unique respite from the radiation effects around Jupiter on its leading, anti-Jovian quarter, this is discussed further in section 4.2.2. Combining this with the protection from the Sun's harmful radiation through the magnetosphere of Jupiter, as also discussed in section 4.2.2, Europa is therefore relatively habitable for a crew of astronauts for the required 196 day period.

1.2.5 Ganymede

Similarly to Europa, Ganymede's surface is also entirely covered in an ice crust, however, there is not as much evidence for a subsurface liquid ocean. There are fewer lineae on the surface of

Ganymede and fewer geological features across the moon. This is thought to be due to the lack of tidal forces upon the dense core as a result of its orbital radius. Additionally, as it is the largest of the Galilean moons, there are no other larger objects to oppose Jupiter's gravitational force and therefore, much less frictional heating. Ganymede therefore offers fewer scientific research opportunities.

1.2.6 Callisto

Callisto is the farthest, regular orbiting moon of Jupiter. In comparison with the inner three Galilean moons, Callisto offers very little for scientific research. It does contain water ice within the rocky surface, however, there is very little to no chance of any liquid water. Callisto displays an impressive array of craters, but after this there is little of interest about this moon.

1.3 Target Selection

In consideration of the above, I propose Europa as the primary destination for a human mission to the Jovian system. The combination of a relatively safe radiation environment and numerous scientific goals provides exemplary reasons above the others. However, as a contingency to Europa, Ganymede offers an excellent secondary target should anything throughout the mission prevent the primary target from being attainable. As the spacecraft will have the specifications required for a mission to Europa, any alterations to the mission will require no additional radiation shielding, life support or fuel. Therefore, a secondary mission can be conducted safely as well as maintaining the ability to conduct scientific research.

2 Mission Outline

2.1 Mission Pre-Summary

In the following sections I summarise the mission outline to the Galilean moon, Europa. I propose my preferred logistical techniques involving the trajectory calculations and the methods of shielding the crew from radiation. As well as the approach I propose to use to support the lives of the crew on board the spacecraft for the duration of the mission. I also consider the optimum way of safely landing on Europa and outline scientific goals of the mission.

In my proposal I assume that the spacecraft is being assembled in Low Earth Orbit (LEO), and as such I propose that the spacecraft be comprised of modules, each with dimensions based on the payload volume of the Falcon 9 Heavy rocket, SpaceX (2009). Secondly, I assume that cost is not a limiting factor, however, at the end of the proposal I will consider the approximate cost of the mission. Finally, in order to reduce the requirements of the spacecraft to ensure fuel and mass costs are as low as possible, I will take as few astronauts as possible. I therefore nominate to take a crew of six astronauts in order to allow three teams of two. In the case of an accident to one of the crew members, the other in the team member is able to report it and take over their roles and responsibilities. Additionally, only one of the teams will land on Europa, while the other two remain in orbit to maintain a human presence on board the main spacecraft at all times.

3 Trajectory

When calculating trajectories to a celestial body one must start from the initial position, in this case, Earth. To escape Earth's gravitational pull the spacecraft must reach escape velocity. Escape velocity is the velocity that if given to an object, the object would have enough kinetic energy to escape the gravitational pull of the massive object, i.e. Earth. The velocity of this object would never reach zero and therefore be able to travel to infinity with respect to that massive object. Infinity with respect to a massive object is defined as at the radius of its sphere of influence at which point it no longer exerts any gravitational forces.

$$V_{esc} = \sqrt{\frac{2GM}{r}} \tag{1}$$

where V_{esc} is the escape velocity to infinite, G is the Gravitational Constant, M is the mass of the central body and r is the distance from the body.

Escape velocity for a massive object can be calculated using equation (1). For Earth this velocity is 11.186 km/s, Williams (2016) from the surface and is 10.790 km/s in Low Earth Orbit, Williams however in low earth orbit a spacecraft is already travelling with a velocity of 7.79 km/s at an altitude of 200 km which means that a much smaller ΔV is required to reach escape velocity. Where ΔV is the change in velocity.

3.1 Trajectory Calculations

In order to effectively calculate the trajectory I made some assumptions: Firstly, I assumed that the solar system was coplaner, allowing me to ignore the relative inclination between Earth and Jupiter's orbits. In practice this would have to be taken into account, however, the ΔV that would be required is negligible and can be included within the initial burn or through in-flight trajectory corrections during the mission, the fuel cost of which will be absorbed by the 10% additional fuel I plan to take. Secondly, I have assumed that the orbits of Earth and Jupiter are circular. This allows me to assume the most efficient Hohmann transfer. In practice, this would also have to be taken into account, changing the ΔV of the initial burn and therefore altering transfer time and launch alignment. A Hohmann transfer uses a primary burn and a secondary burn, the primary occurring from Low Earth Atmosphere (LEO) and the secondary occurring at capture. The ΔV required for the initial and final burns are calculated in equations (2) and (3) respectively. The derivations of these equations can be found in Appendix C.2

$$\Delta V_1 = \sqrt{\frac{\mu}{r_1}}\left(\sqrt{\frac{2r_2}{r_1 + r_2}} - 1\right) \tag{2}$$

$$\Delta V_2 = \sqrt{\frac{\mu}{r_2}}\left(1 - \sqrt{\frac{2r_1}{r_1 + r_2}}\right) \tag{3}$$

Where $\mu = GM$, G = gravitational constant, M = Mass of orbiting body (assuming $M >> m$), r_1 = is the radius of the initial circular orbit and r_2 is the radius of the final circular orbit.

These two equations are derived by calculating the difference in velocity of the elliptical transfer orbit and the velocity of the circular orbit at radii r_1 for initial and r_2 for final. Where the semi-major axis of the elliptical orbit is defined as $a = (r_1 + r_2)/2$ and the velocities are calculated using the Vis-Viva equation, equation (4).

$$v^2 = \mu\left(\frac{2}{r} - \frac{1}{a}\right) \tag{4}$$

I calculated the Hohmann transfer burns to require a ΔV of $\Delta V_1 = 8.790$ km/s and $\Delta V_2 = 5.643$ km/s. The total ΔV required is therefore $\Delta V_{tot} = 14.434$ km/s. In this mission the spacecraft begins by orbiting Earth, as I have assumed the spacecraft is initially in a LEO. Therefore,

the spacecraft will follow a hyperbolic escape trajectory to leave Earth's sphere of influence. A hyperbolic escape trajectory is an orbit with eccentricity > 1 such that the velocity of the object is sufficient never to return to the sphere of influence. The burn required for a hyperbolic escape trajectory can be calculated by knowing the velocity that the spacecraft must be traveling at, with respect to the Earth, at the edge of Earth's sphere of influence in order to be on the correct elliptical orbit; this velocity is known as the hyperbolic excess velocity (V_{exc}). Escaping LEO and entering the elliptical transfer orbit can be achieved simultaneously, where the hyperbolic excess velocity matches the insertion velocity, ΔV_1. Therefore, the velocity of the spacecraft in LEO and the escape velocity (V_{esc}) from LEO we can calculate the required ΔV by using equation (5).

$$\Delta V_\pi = \sqrt{\Delta V_{exc}^2 + \Delta V_{esc}^2} - V_{LEO} \tag{5}$$

Therefore, the initial burn from LEO is $\Delta V_\pi = 6.306$ km/s and from this I am able to calculate the eccentricity of the hyperbolic escape trajectory to be $e = 2.2663$ using equation (6).

$$e = 1 + \frac{r_p v_{\text{inf}}^2}{\mu^2} \tag{6}$$

Where r_p is the periapse of the trajectory, Low Earth orbit in this case.

By knowing the eccentricity of the escape trajectory, I am able to calculate the angle at which the burn must be executed with respect to the Earth in equation (7)

$$\frac{\delta}{2} = \sin^{-1}\left(\frac{1}{e}\right) \tag{7}$$

Where $\frac{\delta}{2}$ is the angle in the direction of the orbit that the final escape velocity vector will possess, this is seen in figure 2. For the initial burn this was found to be $\frac{\delta}{2} = 26.18°$.

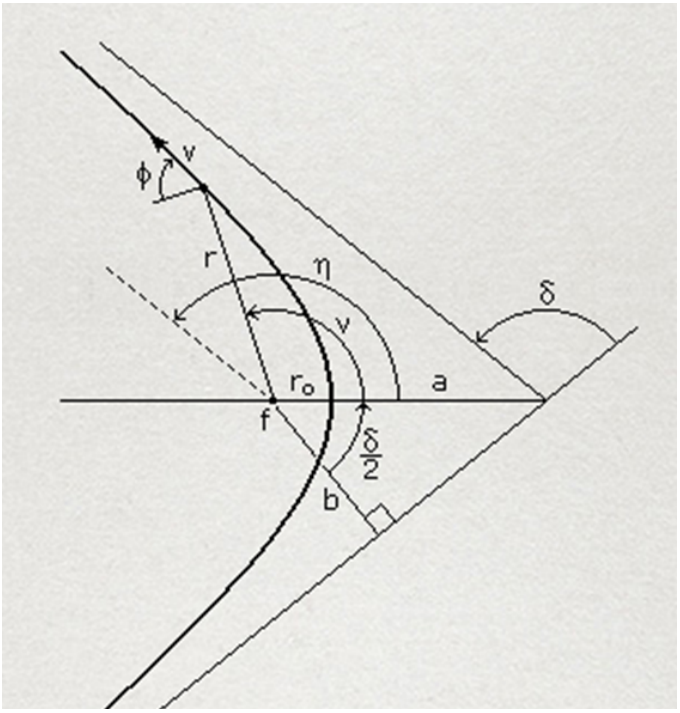

Figure 2: This Figure shows a hyperbolic orbit. The same orbit is applied to both escape trajectories and capture trajectories. Courtesy of Braeunig (2013)

Calculating the hyperbolic capture burn uses the same method, but simply in reverse. The results of this are $\Delta V_\alpha = 6.143$ km/s giving a new overall ΔV of $\Delta V_{tot} = 12.450$ km/s and an angle to the hyperbolic capture periapse of $\theta = 57.3°$, with an impact parameter (perpendicular distance from Jupiter) of $b = 2.558 \cdot 10^9$ km to give a periapse of $r_p = 670900$ km which is the orbit of Europa where a final burn of $\Delta V_F = 1.432$ km/s is required to be captured by Europa's gravity at an orbit of 100 km.

An additional, important factor to consider is the launch alignment. This is the required angle between the two planets such that when the spacecraft arrives at Jupiter's orbital radius, Jupiter is at the correct position. If this was not considered then if you aim for Jupiter, by the time you get there it will have moved and the spacecraft will not be able to catch it up. In order to calculate the alignment I used the following equation, as derived in Appendix C.3:

$$\alpha = \pi \left(1 - \frac{1}{2\sqrt{2}} \sqrt{\left(\frac{r_1}{r_2} + 1 \right)^3} \right) \tag{8}$$

This angle is defined as the angle with which the target planet must be aligned such that in the time taken for the Hohmann transfer the target is at the same position as the rocket. This time is calculated using:

$$t = \pi \sqrt{\frac{(r_1 + r_2)^3}{8\mu}} \tag{9}$$

The transfer time is found to be $t = 86081401$ s which equates to $\approx$2.72 years.

For a Hohmann transfer between Earth and Jupiter, the angular alignment of the two planets must be $\alpha = 153.6°$ for an encounter. The alignment of the planets for the return trajectory is similarly calculated to be $\alpha_{return} = -83.3°$. These alignments give rise to the concept of launch windows. After arriving at the Jovian system there is a very specific time that one must remain there before the return launch alignment is correct. This length of time has been calculated to be 197.33 days. The total length of the mission can then be calculated to be 2189.958 days, which is within one hour of 6.00 years.

The final effect to consider is the Oberth effect, this effect is a bonus to the final velocity of a rocket when a thrust is applied within the gravitational well of a planet. This is because when a rocket is moving with a greater velocity the rocket propellant possesses kinetic energy such that it provides a larger momentum boost to the rocket when exhausted. Therefore, the most efficient time to burn is at maximum velocity, giving rise to the manoeuvre known as an Oberth manoeuvre. This is when a rocket dips into the gravitational well of a body, gaining kinetic energy from the potential as it approaches the planet. At the point of closest approach, with maximum velocity, the rocket burns its fuel, gaining a velocity boost factor. This factor is shown below:

$$\Delta V_{final} = \sqrt{1 + \frac{2V_{esc}}{\Delta V}} \Delta V \tag{10}$$

Therefore, I calculated the Oberth Factor, the ratios between the ΔV after the Oberth effect and before, to be 1.0468 at LEO of Earth such that the hyperbolic capture and escape burn is now $\Delta V_\pi = 6024.4$ km/s and the Oberth Factor at a Europa Orbital radius of Jupiter to be 2.6496, such that the hyperbolic capture and escape is now $\Delta V_\alpha = 2318.7$ km/s.

The return transfer has the same ΔVs, but executed in retrograde, the total ΔV_{Tot} for the entire trip is therefore $\Delta V_{Tot} = 19551$ km/s. As a precaution, I increase this value by 10% to account for any unforeseen trajectory corrections and manoeuvres, giving a final value of $\Delta V_{TotFinal} = 21506$ km/s.

3.2 Trajectory Simulation

In order to confirm that my calculations were correct, I have written a MATLAB simulation of a Hohmann transfer using a 4th order RungeKutta approximation method, Lubich and Ostermann (1995); The main code and functions can be found in appendices B.1 and B.2 respectively. The simulation uses dimensionless variables (Denoted by $\widetilde{}$) that are calculated for each variable as shown below:

$$\widetilde{M_x} = \frac{M_x}{M_{Earth} + M_{spacecraft}} \tag{11}$$

Where $M_{Earth} + M_{Spacecraft} = m$ from this point onwards.

$$\widetilde{V_x} = \frac{V_x}{\sqrt{Gm/a}} \tag{12}$$

Where a = initial separation of spacecraft and Earth (to Earth's centre).

$$\widetilde{R_x} = \frac{R_x}{a} \tag{13}$$

$$\widetilde{t} = \frac{t}{\sqrt{\frac{a^3}{Gm}}} \tag{14}$$

By considering the gravitational forces each body in the system experiences I derived an equation of motion using:

$$F_{tot} = m\frac{d^2x}{dt^2} \tag{15}$$

$$M_{space}\frac{d^2x_{space}}{dt^2} = \frac{GM_{space}M_J}{|r_J^3|}\vec{r}_J + \frac{GM_{space}M_E}{|r_E^3|}\vec{r}_E - \frac{GM_{space}M_S}{|r_S^3|}\vec{r}_S \tag{16}$$

Where a subscript J denotes Jupiter, E denotes Earth, S denotes Sun and space denotes the spacecraft. $|r|$ is the magnitude of the separation and $\vec{r}$ is the vector separation.

Normalizing to be dimensionless, I simply get:

$$\frac{d^2\widetilde{x}_{space}}{d\widetilde{t}^2} = \frac{\widetilde{M}_J}{|\widetilde{r}_J^3|}\widetilde{\vec{r}}_J + \frac{\widetilde{M}_E}{|\widetilde{r}_E^3|}\widetilde{\vec{r}}_E - \frac{\widetilde{M}_S}{|\widetilde{r}_S^3|}\widetilde{\vec{r}}_S \tag{17}$$

Using the same method for the Earth and Jupiter, but reducing to only the gravitational force due to the Sun, by the assumption that the other forces are negligible, I get:

$$\frac{d^2\widetilde{x}_E}{d\widetilde{t}^2} = -\frac{\widetilde{M}_S}{|\widetilde{r}_S^3|}\widetilde{\vec{r}}_S \tag{18}$$

$$\frac{d^2\widetilde{x}_J}{d\widetilde{t}^2} = -\frac{\widetilde{M}_S}{|\widetilde{r}_S^3|}\widetilde{\vec{r}}_S \tag{19}$$

Although not strictly true, the Sun is assumed to be motionless as $M_S >> M$ of any other body in the system. In reality, Jupiter does cause a movement in the Sun's position, but this can be assumed to be negligible.

The equations of motion are used within the function to iterate the position of the bodies by assuming $\frac{dx}{dt} = v$ and $\frac{dv}{dt} = \frac{d^2x}{dt^2}$ i.e. the change in position is v and the change in velocity is $\frac{d^2x}{dt^2}$.

The initial conditions are as follows:

For Earth:

$$\widetilde{x} = |\widetilde{r}_S| \tag{20}$$

$$\widetilde{y} = 0 \tag{21}$$

$$\widetilde{v}_x = 0 \tag{22}$$

$$\widetilde{v}_y = \widetilde{v}_{Eorb} \tag{23}$$

For the Spacecraft:

$$\widetilde{x} = \widetilde{x}_E + \widetilde{a} \cdot \cos(-\beta) \tag{24}$$

$$\widetilde{y} = \widetilde{a} \cdot \sin(-\beta) \tag{25}$$

$$\widetilde{v}_x = -\widetilde{v}_{Spaceorb} \cdot \sin(-\beta) - \widetilde{V}_\pi \cdot \sin(-\beta) \tag{26}$$

$$\widetilde{v}_y = \widetilde{v}_{Eorb} + \widetilde{v}_{Spaceorb} \cdot \cos(-\beta) + \widetilde{V}_\pi \cdot \cos(-\beta) \tag{27}$$

For Jupiter:

$$\widetilde{x} = |\widetilde{r}_S| \cdot \cos\left(\frac{3\pi}{2} - \alpha\right) \tag{28}$$

$$\widetilde{y} = |\widetilde{r}_S| \cdot \sin\left(\frac{3\pi}{2} - \alpha\right) \tag{29}$$

$$\widetilde{v}_x = -\widetilde{v}_{Jorb} \cdot \sin\left(\frac{3\pi}{2} - \alpha\right) \tag{30}$$

$$\widetilde{v}_y = \widetilde{v}_{Jorb} \cdot \cos\left(\frac{3\pi}{2} - \alpha\right) \tag{31}$$

Where subscript Eorb denotes the orbital velocity of Earth, subscript Jorb denotes the orbital velocity of Jupiter, subscript Spaceorb denotes the orbital velocity of the spacecraft at LEO, α is the hyperbolic angular alignment and β is the Launch alignment.

The code runs through a timescale determined by the transfer times calculated in the previous section. Figures 3, 4 and 5 plot the dimensionless x position of the bodies against their dimensionless y positions. The three figures confirm that the previous section's calculations yield the correct values for a Hohmann transfer from Earth to Jupiter. The initial burn has been included into the initial conditions, before the initial point in figure 3 the spacecraft would be on a circular orbit of Earth. The secondary burn is shown in figure 5 at the point the trajectory changes direction. From this point onwards the spacecraft's trajectory is of a circular orbit at the orbital radius of Europa. Figure 4 shows that the angular separation of the two planets is correct, it also shows that the initial burn gives the spacecraft the correct velocity to be put onto an elliptical transfer orbit to Jupiter's orbital radius.

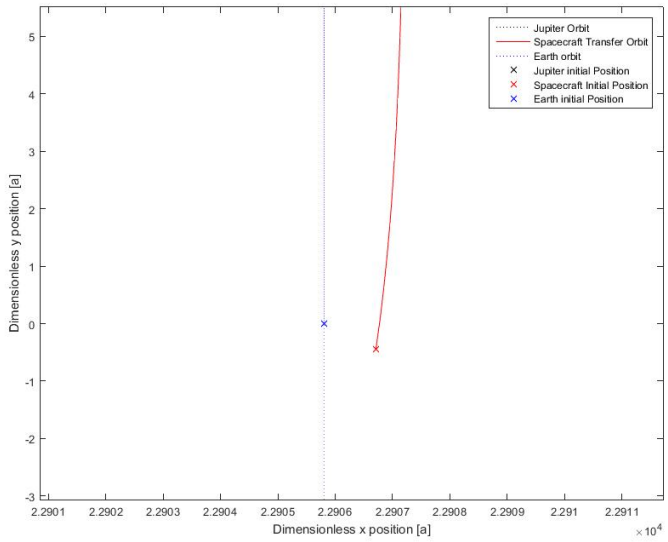

Figure 3: This figure shows the hyperbolic escape trajectory of the spacecraft in a MATLAB simulation

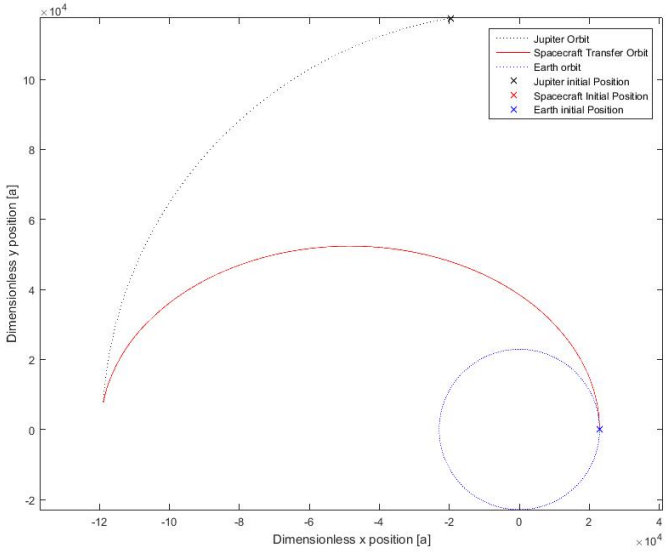

Figure 4: This figure shows the Hohmann transfer trajectory in a MATLAB simulation

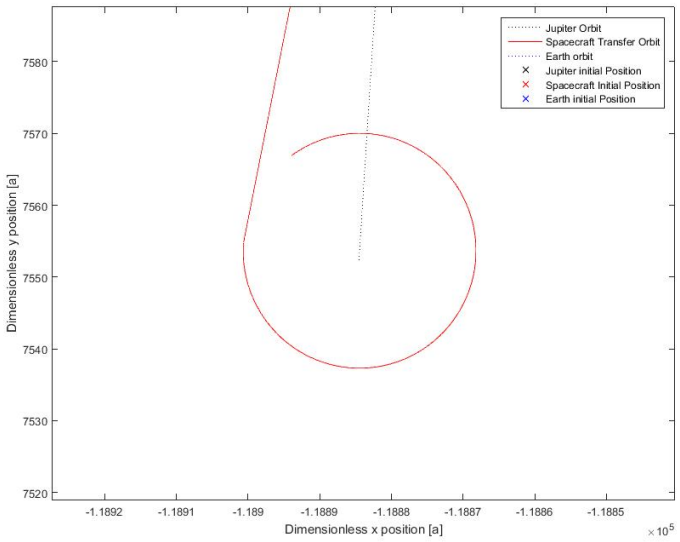

Figure 5: This figure shows the capture trajectory in a MATLAB simulation

4 Radiation

The hazards of radiation during spaceflight are one of the biggest factors in the planning of human missions. Sources of radiation are continuously bombarding the spacecraft throughout the mission. Different periods of the mission pose different types of radiation, requiring multiple layers of protection to ensure that at any point the safety of the crew and equipment is conserved.

Radiation is often classified into ionizing and non-ionizing categories: Ionizing radiation consists of incident particles or photons with energy high enough to break chemical or atomic bonds, causing the target particle to lose or gain an electron causing it to become charged. Non-ionizing particles and photons are those with insufficient energy to ionize but still contribute energy in the form of heat.

In the following sections I provide a background into the types of radiation that will be encountered during the mission and the preventative measures taken to create a safe environment in the spacecraft.

4.1 Ionizing Radiation

Ionizing radiation is the main type of radiation to consider during space flight, the three main types of ionizing radiation are examined in the following sections.

4.1.1 Alpha Particles

Alpha particle radiation is the emission of a helium nucleus; 2 neutrons and 2 protons. Alpha emission is the most ionizing type of emission as it is the most massive particle and therefore has the ability to break off electrons from particles with lower velocities. As a consequence of alpha emission being the most massive, it is also the most easily absorbed. Radiation shielding as thin as paper would be sufficient to shield from alpha emission, Turner (2007).

4.1.2 Beta Particles

Beta radiation is the radiation of high energy, high velocity incident electrons. The smaller cross section of electron interactions allows for deeper penetration into a material. Due to the charge of beta radiation it is more easily decelerated through electromagnetic interactions than photons. As the electron is decelerated, the change in acceleration can give rise to the emission of a photon through Bremsstrahlung.

4.1.3 Electromagnetic Radiation

Ionising Electromagnetic (EM) radiation consists of energetic photons that have sufficient energy to excite particles and therefore influence the composition of the particle. There are three types of ionising electromagnetic radiation: gamma rays, x-rays and ultraviolet rays. Gamma rays are photons that are produced by the nucleus of a particle where as x-rays are produced through the de-excitation of an electron, i.e. Bremsstrahlung, and ultraviolet radiation (UV-rays) is produced by blackbody emission of hot objects; a blackbody is an object that emits isotropically at thermal equilibrium. The wavelengths of gamma rays are the shortest, however they possess the most energy and the wavelengths of UV rays are the longest but possess the lowest energies.

To shield from EM radiation requires objects with a large atomic number density, i.e. dense materials. This is because of the low cross section of EM radiation which allows them to penetrate deeper into materials. Therefore denser materials are required to reduce the mean free path of the photons.

4.2 Radiation sources

There are four main radiation sources whose effects will have implications on a human mission to the outer solar system. These are: the radiation belts within the magnetospheres of Earth and Jupiter, galactic cosmic radiation in the form of cosmic rays and solar radiation emission known as solar weather and solar events. These four regions are discussed in the following four sections.

4.2.1 Earth's Radiation Belts

Earth's radiation belts are generated by the rotation of Earth's core. The rotation of the core creates co-rotating electrical currents that induce a magnetic field around the planet with magnetic field lines creating loops between the north and south poles of the planet, similar to a bar magnet. It is these magnetic field lines that protect the Earth from harmful radiation such as solar radiation and galactic radiation. The interaction between incident radiation and the magnetic field forms a shock front that deflects the radiation along the magnetic field lines towards the poles, leading to the Aurora Borealis and the Aurora Australis as the radiation interacts with the atmosphere. Not all of the radiation is deflected however, some particles are trapped within the magnetic field lines to create what is known as the Van Allen belts. These Van Allen belts are in the shape of a torus and contain high energy electrons. The region where the Earth's magnetic field is dominant and where these effects take place is known as its magnetosphere, any object with a strong enough magnetic field possesses a magnetosphere.

There are two known Van Allen belts the nearest point of which, known as the South Atlantic Anomaly, is at an altitude of 200 km, as highlighted in Figure 6. The inner radiation belt contains a stable population of electrons with energies of a few 100 KeV and protons of energies up to 50 MeV. The outer radiation belt, however, only contains electrons with energy up to 10 MeV, Lee (2014). The outer radiation belt is effected more easily by solar events and galactic cosmic radiation so fluctuates in electron density and energies are created.

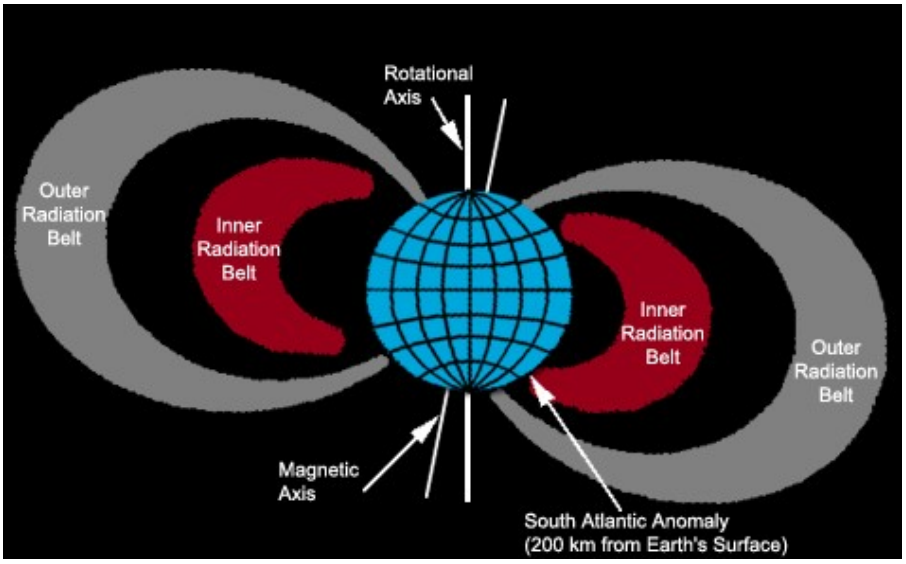

Figure 6: This figure shows the two Van Allen belts around Earth, courtesy of, Lee (2014)

4.2.2 Jupiter's Radiation Belts

As opposed to Earth, Jupiter's radiation belts are generated through the rotation of its outer core, due to its gaseous nature. The magnetosphere of Jupiter is the largest known structure in the solar system, after the heliosphere; the Sun's equivalent magnetosphere. If Jupiter's magnetosphere emitted visible radiation it would appear 2 to 3 times as big in the sky as the Sun or Moon in our night sky.

The structure of Jupiter's Magnetosphere has several key features to consider and can be seen in figure 7. Firstly, external to the magnetosphere itself lies the Bowshock region. This is the region at which solar winds first interact with the magnetic field and are first deflected along the magnetic field lines and around the planet; it has the densest solar plasma. Between the bowshock and the magnetopause, as defined later, lies the magnetosheath, this region's magnetic field lines are easily distorted by solar weather and as a result it contains fewer trapped particles than in the bowshock; this region is known as a transitory state. The magnetopause is the boundary between the surrounding plasma and the magnetosphere, the magnetosphere is defined as the region where magnetic field of the planet dominates and allows regular magnetic field lines, unaltered by solar weather, to form, protecting the planet from radiation. The radius of the magnetosphere fluctuates as a direct result of solar weather on the magnetopause. As the pressure of solar wind increases on the magnetopause, the radius of the magnetosphere shrinks and as the solar pressure diminishes, the radius of the magnetosphere will increase. Within the magnetosphere lies the belts of trapped, high energy particles along the inner magnetic field lines that change very little with solar weather. Finally, on the far side of the magnetosphere, with respect to the Sun, there is the magnetotail. This region consists of high energy protons and electrons, separated by a plasma sheet. This is the region that is mostly responsible for the northern and southern auroras and can reach great radii due to the lack of effects of solar weather.

The radiation belts are created in the same way as the Van Allen belts around Earth, by the Solar winds that get trapped at different magnetic field lines. Jupiter's moon Io is extremely geologically active and as a result plays a large part in the types of radiation within the inner torus. This inner torus is formed through the ejection of sulphur dioxide that is ionized through photoionization by UV radiation from the Sun and Jupiter. Emitted electrons may further ionize the neutral constituents of the torus if their energy is sufficient. As a result the Io torus is a significant source of radiation, especially for Europa as it lies within this torus. The energies of

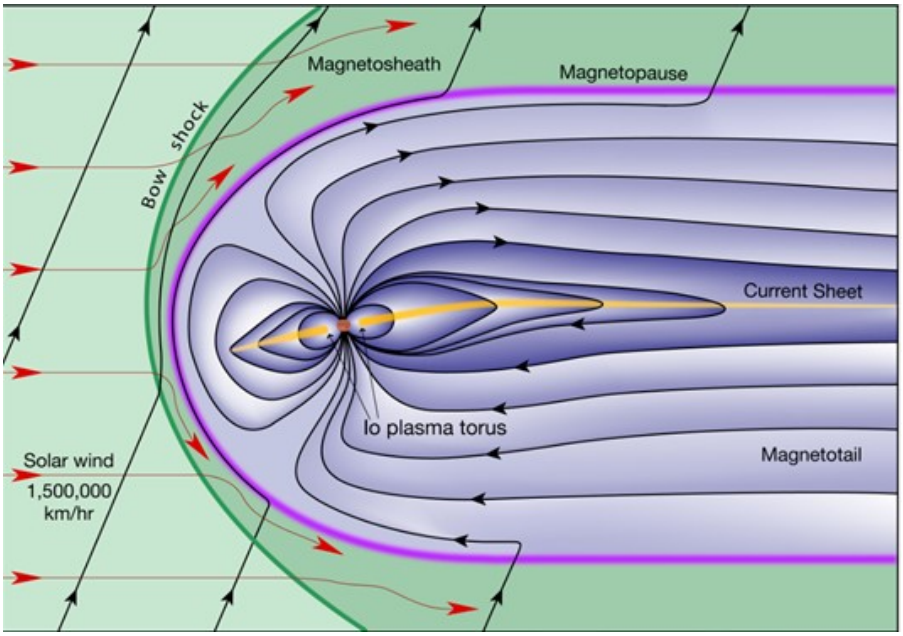

Figure 7: This figure shows the features of the magnetosphere, magnetosheath and bow shock around Jupiter, courtesy of LASP

the plasma of electrons and ions are up to ≈50 MeV, Divine and Garrett (1983).

4.2.3 Galactic Cosmic Radiation

Galactic Cosmic Rays (GCR) are high-speed, fully ionized atomic nuclei that come from outside the solar system, predominantly in the form of alpha particles (99%) from the Milky Way, Berezinskii et al. (1984). As cosmic rays originate outside of the solar system, the quantity within the solar system is determined by the solar cycle. The solar cycle is the cycle of the strength of the Sun that depends upon its magnetic activity, completing one cycle approximately every 11 years, FRIIS-CHRISTENSEN and LASSEN (1991). During a solar maximum the magnetic field is strongest and as a result the heliosphere is at its largest. The heliosphere is the bubble within which solar wind dominates and lies at the point where the pressure of the solar wind is equal to the pressure of the Interstellar Medium (ISM), formed by similar processes to magnetospheres as described in section 4.2.2 and seen in figure 8. When the heliosphere is largest, and therefore strongest, the magnetic field lines are able to trap more of the interstellar wind therefore reducing the GCRs within the solar system.

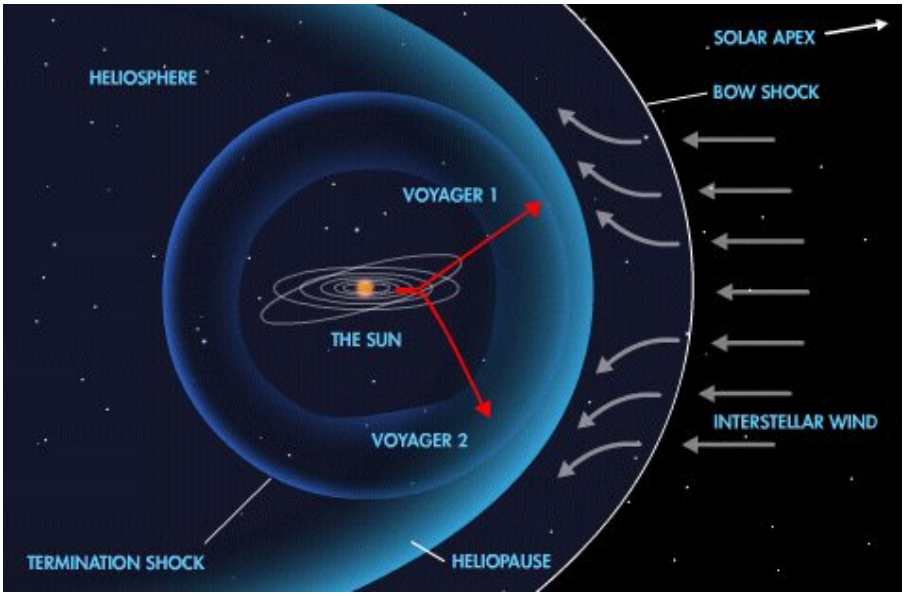

Figure 8: This figure shows the features of the Heliosphere, Heliopause, bow shock and Interstellar wind around the solar system with the trajectories of Voyager 1 and 2 shown, courtesy of LASP

4.2.4 Solar Events

Solar events are the phenomena which occur within the outer atmosphere of the Sun, they include solar wind, solar flares and coronal mass ejections, to name but a few. The primary solar events to consider while planning a mission in space are solar wind and coronal mass ejection as the rest are events within the Sun that do not effect the outer solar system. Solar wind is the constant stream of energetic particles (electrons, protons and alpha particles) emitted from the Sun that form the plasma, filling the heliosphere. Emission of solar wind is at a maximum when the solar cycle is at a maximum and vice versa.

Coronal mass ejections are the large release of plasma from the solar corona. During solar maximum, coronal mass ejections can occur up to three times a day whereas during solar minimum they can occur as little as once every five days, Gosling (2013). On Earth the magnetic field surrounding the planet protects us from these high energy ejections. During interplanetary spaceflight, however, there are no magnetic fields and the spacecraft must therefore be shielded against such radiation.

4.3 Radiation Effects

Radiation affects humans by damaging the DNA within the living cells. When exposed to small doses the cells are able to heal themselves and there are no long term effects. When exposed for a long period of time, or to high intensity radiation the effects can range from the reddening of skin through to the breakdown of intestinal lining that can lead to internal bleeding. The measurement of radiation dosage is measured using two terms: the absorbed dose and the dose equivalent. The absorbed dose can be applied to any type of material and gives a measure of the energy absorbed by that material and has units of Gray (Gy) in SI units. The dose equivalent relates the absorbed dose in human tissue to the effective biological damage of the radiation and has units of Sievert (Sv) in SI units. Different types of radiation have different effects on biological matter and therefore can have a different dose equivalent but the same absorbed dose. The dose equivalent limits for astronauts at skin level over a 30-day period and over their careers are 1.5 Sv and 6 Sv respectively, Townsend (2005). The effects of radiation on biological matter can be split into two categories: stochastic and non-stochastic.

4.3.1 Stochastic Effects

Stochastic effects of radiation are random effects with which the probability of occurrence rises as a function of dose. These effects include cancers, leukaemia and genetic changes. These effects are delayed effects and worsen over time, even in low dose situations. Therefore, when considering a mission with a length of 6 years, the radiation doses received must be kept at a minimum to ensure that astronauts will not suffer from stochastic effects in later life.

4.3.2 Non-Stochastic Effects

Non-stochastic effects are the effects that everyone would experience if exposed to the same doses of radiation. These include radiation sickness, skin reddening, sterility and cataract formation. The main concern for these effects will be within the radiation belts of Jupiter as it is at this time where the largest amounts of radiation must be absorbed, resulting in the requirement for a heavily shielded module.

4.4 Radiation Shielding

In order to ensure that the team of astronauts remain within the safe levels of radiation doses throughout the duration of the mission I propose to use a series of radiation protection methods. For the majority of the mission the spacecraft will be in an orbital transfer. During this time the dominant radiation sources are Galactic Cosmic Rays (GCRs) and radiation from Solar weather. Within the Magnetosphere of Earth and Jupiter the spacecraft is shielded from GCRs and solar radiation but the radiation belts must be considered. The Van Allen belts can be mostly avoided by making trajectory alterations to incline the initial escape to head over the belts before correcting to the original trajectory. This technique can also be applied when traversing Jupiter's radiation belts, however, as Europa lies within one of the belts there must be sufficient radiation protection for this time. Finally, the UV radiation from Jupiter itself must be considered whilst the spacecraft is in orbit around Europa as well as for the base on the surface.

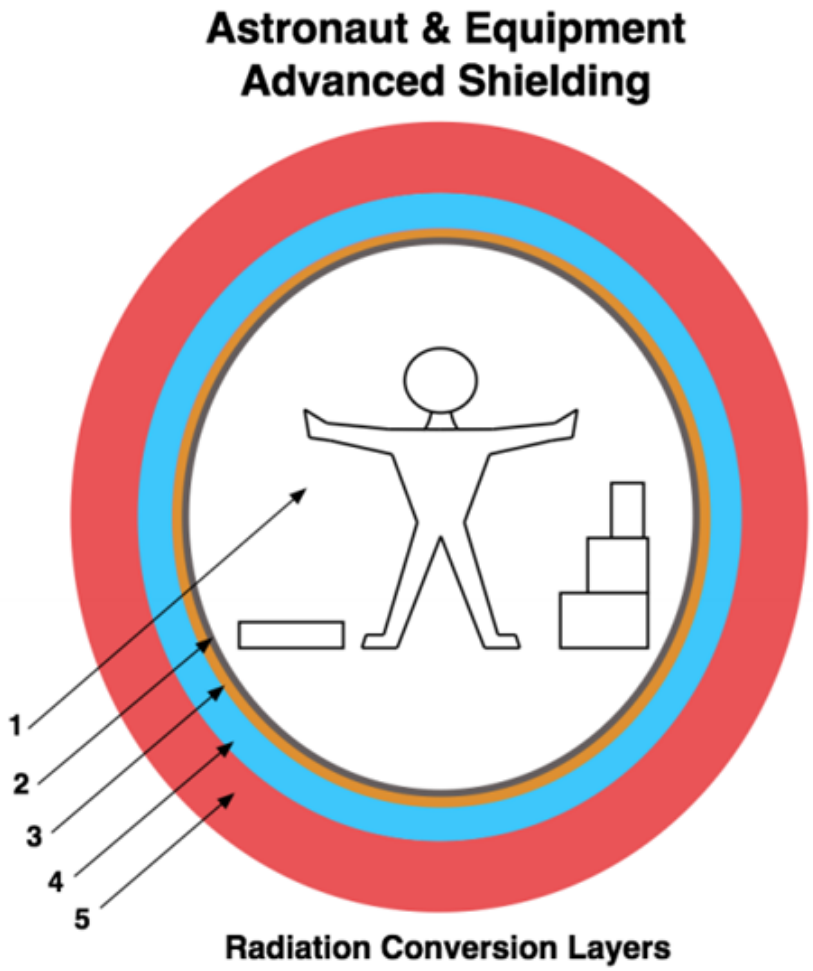

Figure 9: This figure shows the layers of radiation protection, courtesy of Whitney (2016)
Layer 1 is the habitable volume
Layer 2 is the lead layer
Layer 3 is the BNNT composite layer
Layer 4 is the Ionic solution layer
Layer 5 is the Ammonia Borane solution.

As suggested in section 4.3.2 one module will be heavily protected against all forms of radi-

ation by adapting a layered protection set up as shown in figure 9 whilst the remaining living pods only include Layers 3, 4 and 5. I propose this method as for the majority of the spaceflight the main source of radiation will be GCR. However, the bulk of the radiation dose will occur within the radiation belts of Jupiter. Therefore, during this period the crew members on board the main spacecraft will occupy the pod that includes Layer 2 so that they are protected from the high energy electrons and protons. Additionally, should there be any major solar weather events, such as a coronal mass ejection, the heavily shielded pod will give the crew enough shielding to be protected from such an event. Ideally, the entire spacecraft would be protected with all four layers, all being thick enough to shield all radiation, however, as shown in subsection 6.4.3, the mass of shielding one pod alone is extremely high and therefore adds significant fuel requirements.

4.4.1 Ammonia Borane Layer

The use of Ammonia Borane (AB) fulfills both the need for layer 5 and layer 4. Layer 4 will consist of a stable solution of AB and water (pH > 7), Hannauer et al. (2011). AB has a chemical composition H_3NBH_3, Demirci et al. (2011) which has a higher gravimetric hydrogen density than liquid Hydrogen whilst also being stable, non-flammable and non-corrosive. A higher gravimetric hydrogen density is advantageous as it allows for more storage of hydrogen within smaller volumes. The high hydrogen density gives strong radiation shielding against cosmic and solar radiation due to the increased likelihood of an interaction. AB has one additional advantage in that, due to the high hydrogen content, it can be chemically converted into hydrogen fuel through either thermolysis or hydrolysis.

Thermolysis of AB will only start to occur at temperatures of $100°C$ and will not fully decouple until temperatures of $200 - 500°$C, Demirci et al. (2011). Thermolysis of AB yields a gravimetric hydrogen density (GHD) of 13.0 wt%, Demirci et al. (2011) and a gravimetric hydrogen storage capacity (GHSC) of 6.5 wt%, Demirci et al. (2011). Due to the effect of temperature on thermolysis, the AB layer is the inner layer such that it has more heat protection than at the external layer. It should be noted that until it has fully decoupled it is still in a stable, non-flammable state.

As AB is stable in water, a catalyst is required to trigger hydrolysis. This would be in the form of an ionic solution (salt water) i.e. Argon-purged water that is non corrosive to enable safe storage on board a spacecraft. Through hydrolysis at temperatures of 40°C, Demirci et al. (2011) found a GHD of 8.1 wt% and a GHSC of 4.05 wt%. Compared to thermolysis these values are lower, however through hydrolysis greater control over the rate of Hydrogen production is gained as well as the safety benefits due to the lack of reaching the high temperatures thermolysis requires. However, at temperatures of 120° C, thermolysis can be used to recover further Hydrogen after hydrolysis.

Therefore, assuming the use of hydrolysis, layer 5's constituent is an ionic solution. This layer has the ability to slow, breakup and convert particles such that they are more easily shielding in the subsequent layers.

The by-product of hydrolysis will decay into Boron Nitride (BN) crystals; BN has good radiation shielding properties. The crystals could then be used to create further radiation shielding throughout the space flight. This could be used for the lander module, reducing the launch mass whilst giving the same quality of radiation shielding by recycling used fuel.

Finally, as layers 4 and 5 are entirely liquid (before hydrolysis), I propose that they be constructed such that the liquids can be pumped from pod to pod as the crew occupy different pods at different stages of the mission. This allows enhanced radiation protection for a lower overall mass. Leading to drastically reduced costs in radiation shielding, despite the inclusion of a pumping mechanism. The volume of layers 4 and 5 can be found in section 4.4.3, in table 2.

The pumping of fuel through the spacecraft will have effects on the trajectory of the spacecraft, however, as the crew will occupy certain pods for prolonged periods there would only be a small number of exchanges that could easily be corrected using small amounts of fuel. The costs of the extra fuel for corrections would be largely outweighed by the saving on launch mass.

4.4.2 BNNT Layer

Only the Ammonia Borane and the ionic solution layers would be needed if it were not for low energy neutrons. Neutrons have a half-life of slightly over 10 minutes and very low cross sections for interacting with most materials. Consequently, a significant fraction of thermal neutrons can make it into layer 1 unless they are absorbed. In layer 1 the thermal neutrons have the opportunity to interact with tissue, especially the protons in hydrogen, releasing a ≈2 MeV photon, thereby contributing to the radiation dose to the astronauts.

Boron-10 (B-10) has a large cross section for the absorption of thermal neutrons. Previous methods of thermal neutron shielding have consisted of 20% B-10 and 80% B-11, Whitney (2016) and therefore, have had to increase the thickness of layer 3 and layer 4. The solution to this problem is to have as thin a layer as possible with as high a density of B-10 as possible. I propose to use a composite of BNNT, boron carbide (B4C) and epoxy. Boron Nitride Nanotubes (BNNTs) are structural analogues of carbon nanotubes (CNTs) where the Boron and nitrogen atoms have replaced those of the carbon. The advantages are that a BNNT is more thermally and chemically than a CNT, Golberg Et. Al. (2007). The thermal and chemical stability is such that the durability of the proposed composite in space is far superior to CNT and will not degrade during a long mission, Whitney (2016). Additionally, BNNTs have very good radiation shielding properties due to their large thermal cross section. They are also good structural materials and can therefore be used as the main structural component of the spacecraft. For the required radiation shielding of thermal neutrons and GCR a thin layer of hydrogenated BNNT composite would only need be ≈ 1cm thick as outlined in, Whitney (2016). It is this substance that I propose to construct the majority of the spacecraft with to provide the required levels of radiation shielding for the majority of the mission.

4.4.3 Lead Layer

The lead layer makes up layer 2, this layer is required in high energy, ionizing regions. This layer will absorb any radiation the outer layers do not. Therefore It must have a high enough atomic density that it can absorb any electron showers triggered in the outer regions through the absorption of neutrons as well as absorb high energy electrons (up to 50 MeV at Europa's orbital radius) and any massive ionizing particles with energies up to 10 MeV. In order to ensure the maximum safety of the crew I have calculated the thickness of lead required to stop electrons of energies 70 MeV in order to ensure that any energetic anomalies within the radiation belts will also be stopped. I calculated the thickness using the following set of equations, Mahajan (2012):

$$\frac{\mu}{\rho} = \frac{15.2Z^{4/3}}{AE_m^{1.485}} \qquad \frac{\text{cm}^2}{\text{gm}} \tag{32}$$

Where μ is the attenuation coefficient in units of m, ρ is the density of the absorber in units of g/cm^3, Z is the atomic number, A is the Atomic weight in units of u and E_m is the maximum energy of the electron in MeV.

$$\frac{I}{I_0} = e^{-\mu x} \tag{33}$$

Where I has been calculated using the allowed dosage of 1.5 Sv per 30 days of radiation, Rask Et. Al. (2008) and converting into an intensity such that the maximum intensity to pass through the shielding is $I = 3612$ eV/sm^2. I_0 is calculated using the following equation:

$$I_0 = E_m n_e v \tag{34}$$

Where n_e is the electron (plasma) number density in cm^{-3} and v is velocity of the spacecraft moving through the plasma in cm/s and x is the thickness of the shielding material in cm.

At the Europa orbital radius the number density of the plasma has been seen to fluctuate between 30 cm^{-3} and 400 cm^{-3}, Greenberg (2011). The plasma bombards the trailing hemisphere of Europa with a velocity of $\approx$ 100 km/s, Greenberg (2011). As this velocity is far greater than the orbiting velocity of Europa, I have taken this to be the relative velocity of the plasma to the spacecraft. I have calculated the thickness required for different materials in table 1, taking the upper limit of the energies at Europa's orbital radius.

Material	Atomic Weight	atomic number	density g/cm^3	attenuation length (m)	thickness (cm)
Lead	207.2	82	11.36	0.540273146	0.336238043
Aluminium	26.98	13	2.7	0.084616025	2.14687921
Tungsten	183.84	74	19.25	0.899855304	0.201877329
Carbon	12.0107	6	2.25	0.056496585	3.215422402
Iron	55.845	26	7.874	0.300410594	0.604706987

Table 1: This table compares the thicknesses of shielding materials for electrons with Energies of 70 MeV

I am now able to calculate the volumes of each layer, using the payload dimensions of a Falcon 9 rocket, a diameter of 5.2 m and a height of 13.1 m, SpaceX (2009); As shown in Table 2. The most mass efficient material to use for layer 2 is found to be Lead. Additionally, table 3 shows the thickness of lead required as different radii from Jupiter. As the plasma in the Io Torus cools it moves to larger radii, becoming less dense in the process. At the peak energies at a radii of 1 Jupiter Radius R_J the energies are up to 500 MeV and the number density of the plasma as large as 2000 cm^{-3}, Khurana et al. (2004).

Table 3 shows that if the spacecraft were to visit the inner regions of the Io Torus, where the plasma energies and densities are greatest, then the radiation shielding required increases by an order of magnitude. When considering the mass of material required for the thickness of lead required at Europa orbit, the mass of the spacecraft would become far greater than is economically feasible with current launch technologies. The 200 MeV energies correlate to the energies and density of the plasma at the orbital radius of Io, $\approx 6R_J$. Therefore, the spacecraft I propose will not have the capability to visit any regions inwards of Europa, should crew members be aboard.

The remaining volume of the pod is the space that can be utilized for crew members, scientific equipment, life support and controls. The radius and volume of this space is 2.437 m and 244.3 m^3 taken from Table 2.

	Material	Density (Kg/m^3)	Radius Outer (m)	Thickness (m)	Radius Inner (m)	Volume (m^2)	Total Volume (m^3)	Mass (Kg)
Layer 5	Ammonia Borane	780	2.6000	0.1000	2.5000	1.6022	20.9890	16371.40
Layer 4	Ionic Solution	1040	2.5000	0.0500	2.4500	0.7775	10.1858	10593.26
Layer 3	BNNT Composite	1633	2.4500	0.0100	2.4400	0.1536	2.0125	3286.37
Layer 2	Lead	11360	2.4400	0.0034	2.4366	0.0515	0.6748	7665.97
Layer 1	Utility	0	2.4366	2.4366	0.0000	18.6523	244.3448	0.00
Layer 2	Aluminium	2700	2.4400	0.0215	2.4185	0.3277	4.2927	11590.38
Layer 1	Utility	0	2.4185	2.4185	0.0000	18.3761	240.7269	0.00
Layer 2	Tungsten	19250	2.4400	0.0020	2.4380	0.0309	0.4053	7801.53
Layer 1	Utility	0	2.4380	2.4380	0.0000	18.6728	244.6143	0.00
Layer 2	Carbon	2250	2.4400	0.0322	2.4078	0.4897	6.4152	14434.13
Layer 1	Utility	0	2.4078	2.4078	0.0000	18.2141	238.6044	0.00
Layer 2	Iron	7874	2.4400	0.0060	2.4340	0.0926	1.2130	9550.87
Layer 1	Utility	0	2.4340	2.4340	0.0000	18.6112	243.8066	0.00

Table 2: This table shows the thickness of each layer, including the different potential materials for layer 2 and the potential utility volume.

Distance (R_J)	Energy (MeV)	attenuation length (m)	plasma density	thickness (cm)
10	70	0.540273146	400	0.336238043
8	100	0.318114871	800	0.604054146
6	200	0.113646072	1000	1.771477985
2	500	0.029148319	2000	7.458951316

Table 3: This table shows the shielding thickness as the energies and number density of the electrons in the plasma increases.

5 Propulsion

Efficient rockets were developed in the early 20th century through the pioneering work of Konstantin Tsiolkovsky, who developed the Tsiolkovsky Rocket Equation in "The Exploration of Cosmic Space by Means of Reaction Devices" which lead to the work of Robert H. Goddard named "A method of reaching extreme altitudes". His application of the de Leval Nozzle to liquid fuel rockets improved the efficiency of rockets by increasing the exhaust gas velocity to supersonic speeds for liquid monopropellants such that interplanetary space travel became possible.

Since the development of liquid engines there have been many advances in the capabilities of rocket engines as well as many new types of engine being developed, all with particular advantages and disadvantages. In the following section I am going to discuss the different types of engines including liquid fuel engines, solid fuel engines, Ion thrusters, Nuclear engines and experimental propulsion techniques.

5.1 Liquid Fuel Engines

5.1.1 Monopropellant Engines

Monopropellant liquid engines use a single type of fuel that has chemical properties such that when it is combined with a catalyst a chemical reaction is triggered creating the thrust through

the nozzle at the rear of the engine. This can be seen in figure 10. As the propellant is injected into the catalyst bed, a chemical reaction occurs, causing the exhaust gas to choke through the throat of the nozzle gaining velocity into the thrust chamber where it delivers the thrust to the rocket.

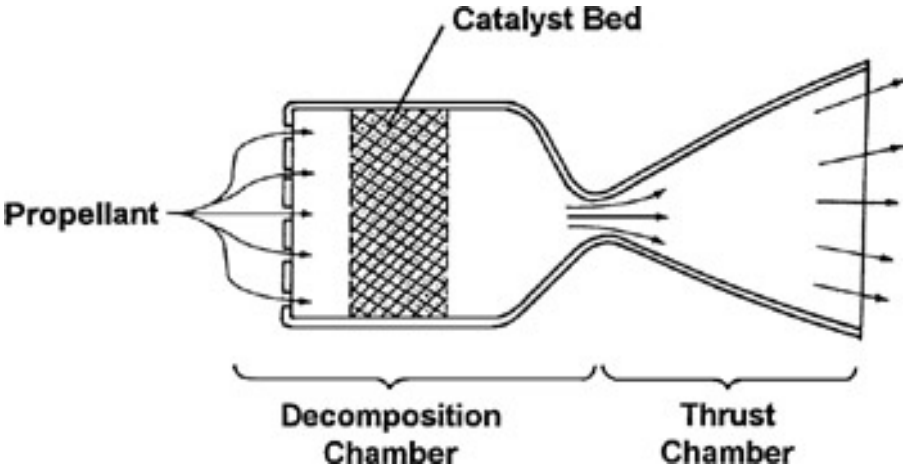

Figure 10: This figure shows the basic schematic for a Monopropellant Engine, courtesy of Brown (2002)

The most common fuel used in these types of engines is Hydrazine (N_2H_4) which is a catalyst of Alumina coated in Iridium. Monopropellant engines are mostly used when there is a need for high reliability without the need for high specific impulse, for example manoeuvring thrusters. There are many other fuels that can be used in monopropellant engines, these, along with their properties, can be found in table 14 of the appendix.

5.1.2 Bipropellant Engines

Bipropellant Liquid fuel engines are different to monopropellant engines as they use a combination of a fuel and an oxidizer to create a thrust by pumping both into a combustion chamber in carefully calculated mixing ratios. This can be seen in the basic schematic of a bipropellant liquid engine in figure 11. There are two tanks, one containing the fuel and the other the oxidizer. Each has a pump that connects them to the combustion chamber at which point the two react to create a hot, high pressured exhaust gas. The gas then passes through the throat of the nozzle creating further acceleration before it exits the engine. Thus, according to Newton's third law a thrust is produced as the momentum of the exhaust is in the opposite direction to the rocket.

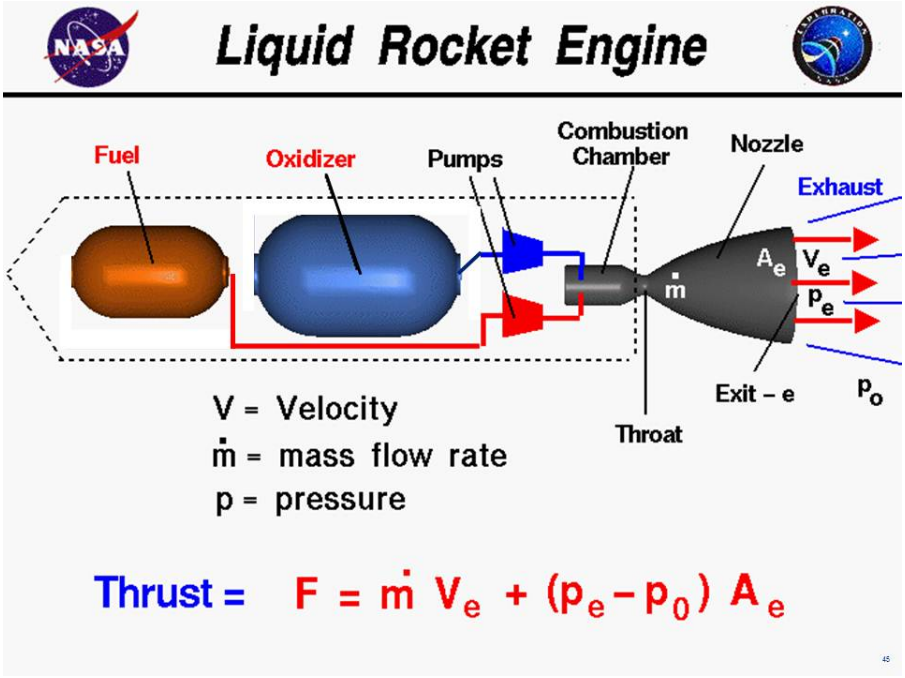

Figure 11: This figure shows the basic schematic for a Bipropellant Engine, courtesy of Benson (2014)

Typical specific impulses for bipropellant liquid engines fall between 311 and 450.5 seconds, SpaceX (2009); Alliance (2010), Merlin 1D and Atlas V engines respectively. However one of the largest advantages to using a liquid fuel engine is that it is able to be throttled, i.e. it can be fired at different specific impulses and can be cut off completely and then restarted. This gives huge bonuses when performing burns as any leftover fuel can be used later in a mission for corrections to trajectory or in a secondary burn.

5.2 Solid Fuel Engines

A solid fuel engine uses similar fuel and oxidizer combinations to that of a liquid fuel engine, however in a solid fuel engine the mixture of fuel and oxidizer is one solid rather than two liquids. The most common fuel used is powdered aluminium which is combined with Oxygen using ammonium perchlorate. This solid mixture is then stored in a cylindrical shape within the rocket such that there is an empty region through its centre that can act like a combustion chamber when ignited. At the top end of the 'combustion chamber' (the left hand side of figure 12) there will be an ignition that ignites the surface layer of the fuel mixture, Dumoulin (1998). The reaction creates hot, pressurized exhaust gas that accelerates through the throat of the nozzle before exiting the rocket giving a thrust, according to Newton's third law.

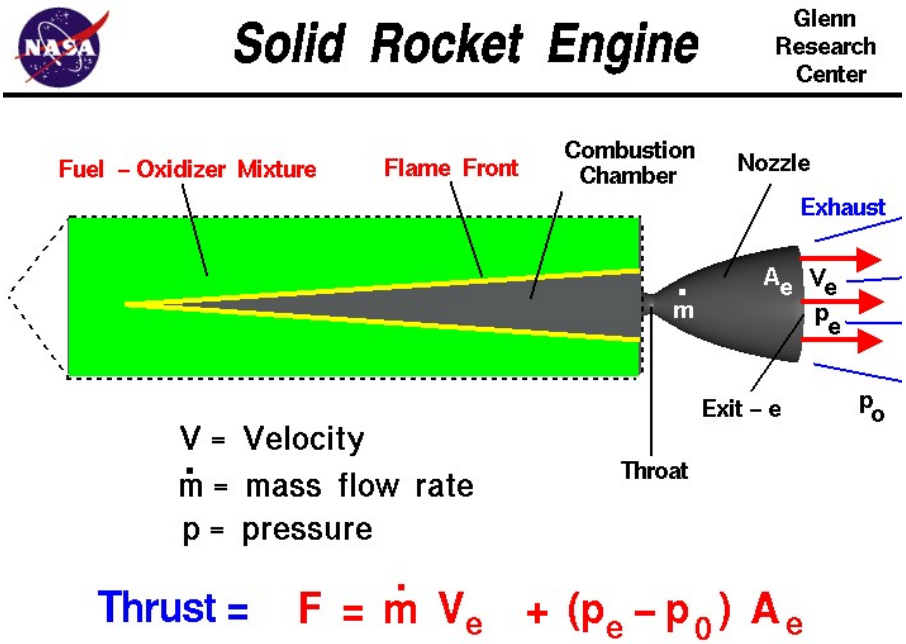

Figure 12: This figure shows the basic schematic for a Solid fuel Engine, courtesy of Hall (2015)

Solid fuel rockets are a cheaper alternative to liquid fuel engines, however they are not as flexible as liquid fuel engines as they cannot be throttled and controlled as easily. For this reason solid fuel engines are mostly used in the initial stages of launch to provide extra lift before detaching in the upper atmosphere.

5.3 Ion Thrusters

Ion thrusters create ions by combining a neutral propellant with electrons. The electrons are generated by thermionic emission, which is when a charged particle can overcome the work function of a material through the thermal energy it is given by the discharge hollow cathode. The electrons emitted by the electron gun are attracted to the discharge chamber walls by a highly charged positive potential. The neutral propellant is fed into the discharge chamber where they can be bombarded by the electrons to create a positively charged ion and electrons. The magnets around the chamber prevent the electrons from freely reaching the discharge channel walls in order to increase the probability of an ionizing event by increasing the time the electrons are within the discharge chamber and therefore increasing their density and the likelihood of a collision. The positively charged ions move towards the back end of the thruster toward the screen grid which contains thousands of precisely aligned apertures to allow particles to pass through. The screen grid has a large positive charge so that once the ions pass through the grid they are rapidly accelerated towards the acceleration grid which has a large negative charge. Through this acceleration, particles can reach velocities of up to 40 km/s. Additionally to this process there is a secondary electron gun, known as the neutraliser, which emits an equal amount of electrons as ions from the thruster in order to neutralise the ions outside the thruster. This prevents the ions from being attracted back towards the thruster and slowing down the spacecraft as well as preventing any spacecraft erosion that may occur from ion bombardment. The process described is illustrated in figure 13.

The favoured propellant for an Ion thruster is Xenon. Xenon is easily ionized and has a high atomic mass which means that when the ion is accelerated there is a greater change in momentum and therefore a greater generated thrust. Additionally, Xenon can be stored at high densities, allowing less volume of propellant to be taken for the same thrust gained. The advantages of these features of an Ion thruster mean that for deep space travel they are ideal. NASA have performed tests on the NEXT Ion thruster for 51000 hours, Van Noord (2007) which shows that NEXT could provide continuous thrust for 6 years of space travel without any noticeable degradation to the thruster. However, despite the NEXT thruster providing a maximum specific impulse of 4100 s, the thrust generated in a vacuum is only 0.236 N, Herman (2010) which in comparison to a Merlin 1D liquid fuel engine that generates 825000 N of thrust, SpaceX (2009) is extremely small. This means that ion thrusters can only be used in orbital transfers and not in initial stages of the rocket. Additionally, because the thrust is so small an orbital transfer manoeuvre cannot be executed with an initial and final burn but with constant corrections to the trajectory throughout the transit.

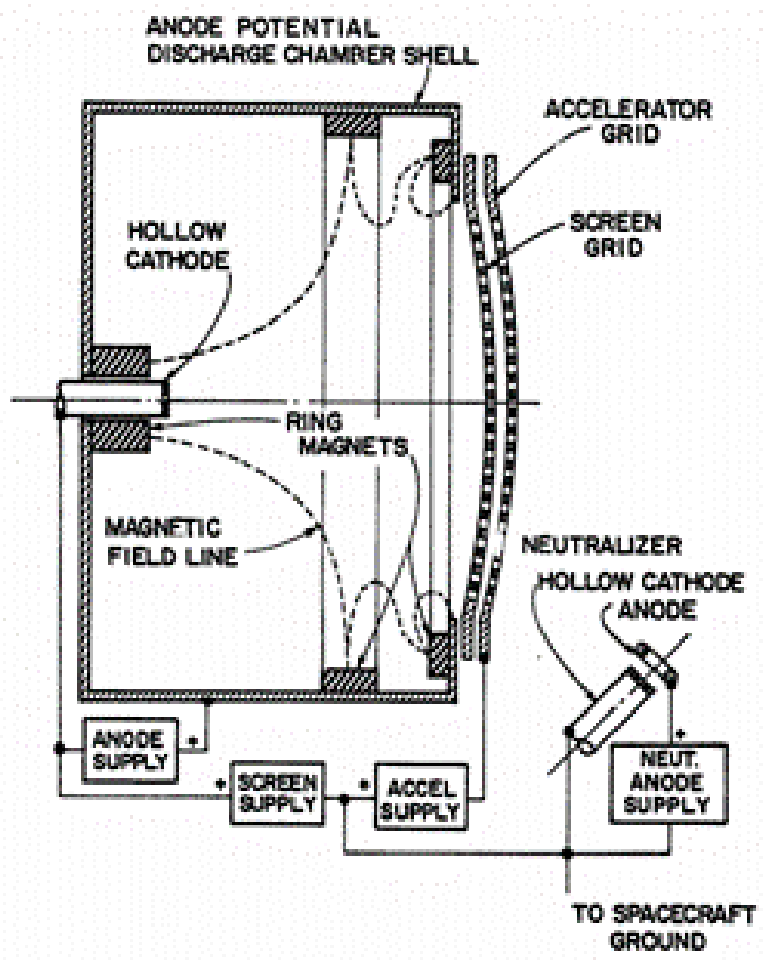

Figure 13: This figure shows the basic schematic for an Ion thruster, courtesy of Brophy (1984)

5.4 Nuclear Engines

Nuclear engines are, at the moment, untested as no space flight has ever been conducted using one. However, nuclear engines could have the potential to double or triple payload mass compared with, currently used, liquid engines, Ragsdale and Willis Jr. (1971). The theory behind a nuclear engine is that instead of using combustion to create an exhaust gas that generates thrust, a nuclear reaction of a fuel component, such as Uranium 235, would be used to emit thermal energy that a liquid propellant would transfer into kinetic energy. Figure 14 shows a schematic of the proposed NERVA nuclear engine. The reactor can be seen in the centre of the rocket, surrounded by the pressure vessel lines that carry the cool propellant from the tank around the nozzle to act as a coolant before gaining the thermal energy from the nuclear process to give kinetic energy to generate a thrust when it exits through the nozzle, Robbins and Finger (1991).

This design was developed during the 1960s before the plans for a manned mission to Mars were set back due to cuts in funding. Despite this, the design was expected to achieve impulses in excess of 800 s, Robbins and Finger (1991), nearly twice as much as the Atlas V liquid fuel engine whilst maintaining thrusts comparable and larger than the liquid engine, Robbins and Finger (1991). This would mean that if the development of a nuclear engine is successful, at the level theorized in the 1960s we could immediately double or triple the payload of a spacecraft if

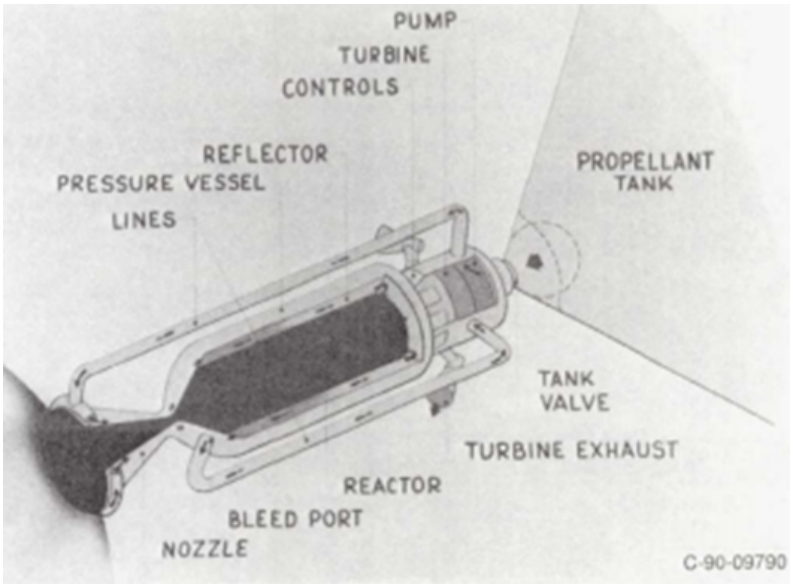

Figure 14: This figure shows the basic schematic for a Nuclear Engine, courtesy of Robbins and Finger (1991)

a nuclear engine was used as an upper stage engine. Additionally, with the higher specific impulse and thrust, one could cut the time of a manned mission through the solar system drastically, assuming the same total fuel mass, such that the radiation effects of space travel would also be cut.

Nuclear engines are perceived have the potential to cause far greater damage to the environment and to those on board a human mission. As there is emission from the radioactive fuel at all times, the spacecraft would need additional shielding for any electronics on board as well as for any humans.

5.5 Proposed Propulsion Method

Through consideration of previous sections, the propulsion method necessary must give a significant ΔV over a relatively short timescale in order for the Hohmann approximation to be true. In order to utilize the Ammonia Borane and Ionic Solution combined yield of Hydrogen I propose to use a liquid fuel engine, using liquid Hydrogen as its propellant. Table 4 lists the liquid fuel engines that use Hydrogen as a propellant.

Engine	Specific Impulse (s^-1)	Exhaust Velocity (m/s)
Vulcain 2	429	4208.49
RL10	465.5	4566.555
J-X2	448	4394.88
RJ-2	421	4130.01

Table 4: shows the specific impulses and exhaust velocities of four Hydrogen based liquid fuel engines.

To the first order, the engine that best fits the needs for this mission is the engine with the highest exhaust velocity. This reduces the mass of the fuel needed to generate the required thrust. However, the thrust to mass ratio must also be considered in order to maximise the efficiency of the mission. Table 4 suggests that the RL10 Engine will be the most efficient engine to use due to its higher exhaust Velocity. In order to check that this is indeed the case, I have calculated the mass ratio of initial and final masses after the burns through the mission. This is independent of the actual mass of the spacecraft and the final payload mass is discussed in section 9.

Final Mass (kg)	Del v (m/s^2)	initial mass (kg)	fuel-mass ratio
Vulcain 2			
1000000	6024	4223305.442	4.223305442
4223305.442	2318	7351905.483	7.351905483
7351905.483	1432	10354458.69	10.35445869
10354458.69	1432	14583268.93	14.58326893
14583268.93	2318	25386469.51	25.38646951
25386469.51	6024	107214814.8	107.2148148
107214814.8	977.4	135446422.9	135.4464229
RL10			
1000000	6024	3740264.55	3.74026455
3740264.55	2318	6213721.535	6.213721535
6213721.535	1432	8502364.554	8.502364554
8502364.554	1432	11633962.45	11.63396245
11633962.45	2318	19327564.14	19.32756414
19327564.14	6024	72290203.02	72.29020302
72290203.02	977.4	89543366.17	89.54336617
J-X2			
1000000	6024	3938050.835	3.938050835
3938050.835	2318	6542304.949	6.542304949
6542304.949	1432	8951972.082	8.951972082
8951972.082	1432	12249169.79	12.24916979
12249169.79	2318	20349611.4	20.3496114
20349611.4	6024	76112930.12	76.11293012
76112930.12	977.4	94278445.6	94.2784456
RJ-2			
1000000	6024	4299901.476	4.299901476
4299901.476	2318	7143449.358	7.143449358
7143449.358	1432	9774530.493	9.774530493
9774530.493	1432	13374693.59	13.37469359
13374693.59	2318	22219450.12	22.21945012
22219450.12	6024	83106621.6	83.1066216
83106621.6	977.4	102941288.6	102.9412886

Table 5: shows the initial mass to final mass ratios for the previously discussed engines.

Table 5 shows that the RL10 engine is indeed the most efficient in terms of the smallest required mass with a ratio of 89.5 compared to the other engines with ratios: 135.4, 94.3 and 102.9. The estimated 1000000 kg is independent of the mass ratio so that for the final mass of the spacecraft, as calculated in section 9, a different engine will not be more efficient.

6 Life Support

In order to support the crew on board the rocket for the duration of the mission efficient recycling of consumed resources is required as there are currently no ways to resupply a mission such as this without incurring significant costs. To do this we must create a closed loop within the spacecraft that recycles required consumables from the waste of other consumables. An example of a closed loop system is shown in figure 15 for NASA's space shuttle, the space shuttle is able to use its fuel cells to generate water by combining Hydrogen and Oxygen to generate electricity. This method of generating electrical energy is far safer than burning the Oxygen. Finally, throughout the discussion of life support, I have included contingency resources so that should the circumstances arise, the crew can be kept alive for longer than the minimum time required.

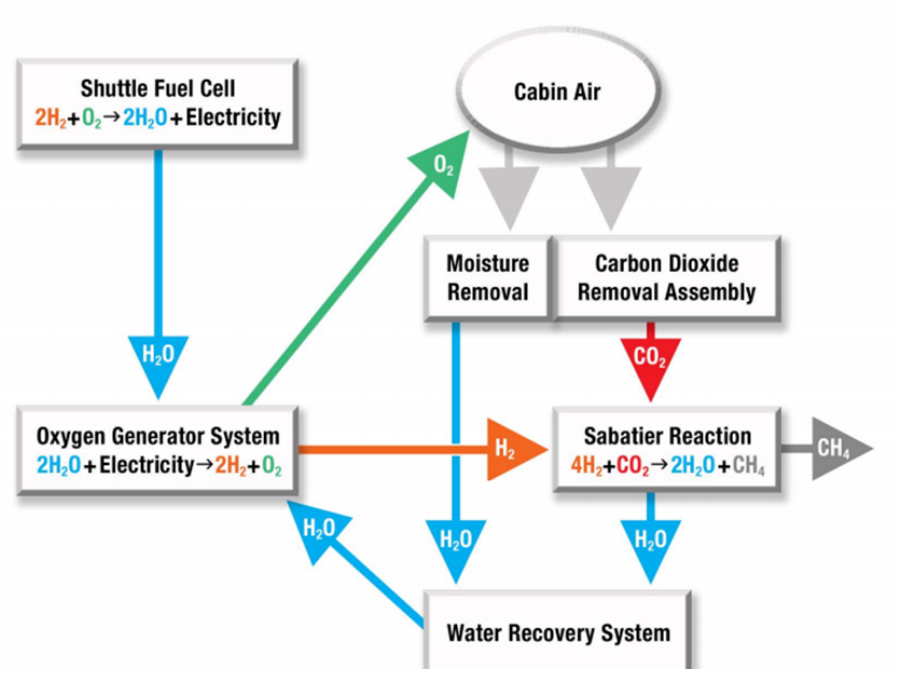

Figure 15: shows the closed life support loop, courtesy of , NASA

6.1 Electricity Generation

The fuel cells I propose to use in this mission are Proton exchange membrane (PEM) fuel cells that are able to produce 20 kW of power for at least 10000 hours, Warshay et al. (1997). To calculate the power required by the spacecraft I have used the same power requirement for the ISS of 75 to 90 kW, Williams Et. Al. (2011). Over a mission length of 6 years (52560 hours) I will need five PEM fuel cells to be producing power continuously, therefore assuming a maximum lifetime of 10000 hours I will need 30 PEM fuel cells on board. The cells will be operating in groups of five for 10000 hours before the next group takes over. This supplies the flexibility should any group fail, others can take their place.

I then calculated the total mass of Oxygen and Hydrogen needed as fuel for the cells are 95406 kg and 14311 kg respectively; this equates to volumes of 83.7 m^3 and 12.5 m^3 respectively. The advantages of using a fuel cell that requires Oxygen and Hydrogen are that the Engine I propose uses the same fuel. In addition, the Ammonia Borane radiation shielding layer is a method of storing Hydrogen efficiently. Furthermore, as the by-product of the fuel cells is water, it removes the requirement for the water to be recycled as there is constantly water being produced through the mission. However, filters will still need to be included to ensure the water is suitable for

drinking.

Finally, additional energy produced will be stored in batteries such that it can be utilized in the case of the fuel cells temporarily failing. This energy can also be used to create oxygen and hydrogen from water should there become a shortage on board.

In further consideration, radioactive thermocoupling generators may provide a superior alternative in terms of total mass including fuel, however, the quantities required for a mission of this length would incorporate taking a mass of isotopes larger than the critical mass. A trade-off between mass and volume therefore ensues.

6.2 Air Environment

I propose that the Air environment aboard the rocket is of a similar composition to that of Earth's atmosphere. The advantages of this mean that the majority of the environment comprises of nitrogen, a stable gas. Using an environment such as on Earth's reduces the fire risk compared to a pure oxygen environment as on the Apollo 1 rocket.

The recycling of air on board the spacecraft will use the same Carbon Dioxide Removal Assembly (CDRA), Trace Contamination Control Subassembly (TCCS) and Major Constituent Analyser (MCA) as on the International Space Station (ISS). The CDRA uses three beds to revitalize the air; the first is a desiccant bed that conditions the air before entering the absorbent bed that contains a CO_2 sorbent to filter the CO_2 overboard, finally, the filtered air is then passed through a second desiccant bed that replaces the humidity in the air. The CDRA system also has a water-save system that can retain the water on board that is removed by the primary desiccant bed. A future development to the CDRA is to vent the CO_2 through a Carbon Dioxide Reduction System to reduce the consumables required in the open-loop system, Sherif and Knox (2005).

The TCCS is used to remove the hazardous trace contaminates in the air through the use of a fixed bed of granular activated Carbon, a thermal catalytic oxidation reactor that leads to a fixed bed of granular Lithium Hydroxide to remove the gaseous acid oxidation by-products from the air stream. The combination of the CDRA and the TCCS are very effective at maintaining a cabin air quality that aligns with the Spacecraft Maximum Allowable Concentration (SMAC) standards. SMAC monitor the maximum allowable contaminants, the full list of allowed values can are found in, NASA (1999).

6.3 Water Recovery Systems

As discussed earlier, the water production on board will be covered by the fuel cells. I propose that the mission uses the Environmental Control and Life Support System's (ECLSS) Water Recovery System (WRS), comprised of the Urine Processor Assembly (UPA) and the Water Processor Assembly (WPA). The WRS also contains an Oxygen Generation System (OGS) where the waste water has its gases removed and is filtered of odour-causing contaminants before returning the generated air to the cabin. The water is then pumped through the OGS, followed by two multi-filtration beds; if the water breaches the first of these beds the second takes its position and a new bed is installed in the second's initial position. In this process, non-volatile organic and inorganic contaminates are removed. Further organics are oxidized and heated before passing through a gas/liquid separator where the excess oxygen is returned to the cabin. Finally, an ion exchange bed removes any dissolved products of oxidization and adds iodine to sterilize the water before the water is stored in the spacecraft's potable water unit, Bagdigian and Cloud (2005).

The WRS is able to recover 70% of the wastewater, Carter (2012). Using the water consumption requirements as shown in table **??** a total water consumption per day of 28.7 kg/person day. Therefore the total mass of water required per astronaut for the duration of the mission is 62853 kg before recycling and 18856kg after including the WRS. Therefore, for a crew number of six this

becomes 113135 kg and finally, adding 10% to account for any unforeseen circumstances the total mass is ≈125000 kg, equating to a volume of 125 m^3. Therefore one module will be designated to water storage.

Consumable	Load (kg/person/day
Oxygen	0.85
Water (Drinking)	1.6
Water (in food)	1.15
Water (clothes and dishes)	17.9
Water (Hygiene)	7.3
Water (Food Prep)	0.75
Food Solids	0.62

Table 6: shows the consumables required by an astronaut in kg per astronaut per day

6.4 Food Supply

When considering the problem of supplying a full nutritious diet to astronauts throughout the mission, one must not only consider the dietary requirements but also the consequences of the food type, for example if crumbs enter the air revitalization system it can cause damage that could lead to failure of the system. If this were to occur halfway through the mission there would not be much chance of receiving aid quickly. Therefore, on board food is stored in a pre-packed dehydrated condition, Perchonok and Bourland (2002). This type of food storage gives the benefit of having less mass than conventional foods as well as occupying less volume. The food is then rehydrated on board, using hot or cold water, depending on the food stuffs. By using this method of storing the food stuffs, I am able to calculate the total mass per person per day, using table **??** I find that this mass is 1358 kg, for a crew of six people this equates to a total mass of 8150 kg.

6.5 Artificial Gravity

Prolonged weightlessness can lead to serious problems in the human body upon re-entry to a gravity field. The loss of bone and muscle, cardiovascular deconditioning, loss of red blood cells and plasma, compromising of the immune system and incorrect interpretation of the Otolith systems (balance systems) are just some of the major effects, Young (1999). This poses large risks for human interplanetary travel. Firstly, due to the lack of artificial gravity research on humans, we are not aware of the level of artificial gravity that would be required to reduce these effects. For example, we do not know whether an artificial gravity of 0.134g (where g is the acceleration due to gravity on Earth, and 0.134g is the acceleration due to gravity on Europa) would be sufficient to reduce any effects of re-entry into the Europan gravity field. However, for the purposes of the following calculations, I am going to assume that an artificial gravity of 0.134g for the duration of the outward flight is sufficient enough to reduce detrimental effects whilst on Europa. During the return transfer, a gradual build up of artificial gravity to 1g will be employed. This ensures a gravity of 1g for the entire year previous to re-entry to Earth's gravity field, therefore building bodily strength and reducing negative effects of re-entry. The weight of items under artificial gravity is due to the Coriolis effect that acts on objects experiencing centripetal force to give them an effective weight. Therefore the astronauts will consider anything they pick up on board to have a weight. The astronauts can therefore exercise as they normally would on Earth throughout the

mission to maintain sufficient bodily strength.

Therefore, in order to create artificial gravity I propose that the spacecraft creates a centripetal force by rotating about its central axis. The modules will therefore be arranged in a circular configuration such that the radius to the centre of the spacecraft is 50 m, therefore being comprised of 24 modules. I propose a 50 m radius in order to reduce the impact of the difference in centripetal force at different radii, for example, if I chose to rotate each module individually about their axis of symmetry, the radius would only be 2.6 m, therefore a crew member of height 1.8 m would experience a difference in gravity of 0.692g. This would mean that when picking objects up the weight of the object would change as you picked it up higher. Using a radius of 50m and an axis of symmetry outside of the modules means that within any one module the gravity force vector is in the same direction and the difference in gravity is only 0.035g. In order to maintain a controlled spin of the spacecraft, the mass of the spacecraft must be configured symmetrically. Therefore, I also propose that parallel with the rotation axis, at the centre of the spacecraft, modules also be aligned that are solely used for fuel storage due the large amounts required, as discussed in section 6.7.

In order for the spacecraft to maintain an artificial gravity of 0.134g on the outwards flight, using equation 36 an angular velocity of 0.0258 rad/s is required, this equates to a rotation of 0.246 rpm.

$$a = \frac{v^2}{r} \tag{35}$$

Such that:

$$\omega = \frac{1}{2\pi} \cdot \sqrt{\frac{a}{r}} \tag{36}$$

Using the above equation, I am able to calculate the required angular velocities required for the variations of artificial gravity up to 1g as shown in Table 7. This table also shows the required mass ratio of spacecraft before and after to accelerate the spacecraft to the required angular velocity. This mass has been calculated using liquid hydrogen as the propellant and simply allowing the pressure it is stored at to act as the accelerator when opened to the vacuum. The first row is the artificial gravity to match that of Europa's and the following mass ratios are the mass ratio to increase the angular velocity from the previous gravity to the new gravity. The total mass required for the rotation of the spacecraft is therefore a maximum of 0.1192 the original spacecraft mass. In practise, this will be lower as the rocket reduces its mass throughout the mission through the expenditure of fuel.

Gravity (g)	angular velocity (rad/s)	Mass Ratio
0.13	0.0258	1.0421
0.2	0.0315	1.0516
0.3	0.0386	1.0636
0.4	0.0446	1.0738
0.5	0.0498	1.0829
0.6	0.0546	1.0911
0.7	0.0590	1.0988
0.8	0.0631	1.1060
0.9	0.0669	1.1127
1	0.0705	1.1192

Table 7: shows the mass ratio required to accelerate the rotation of the spacecraft in order to generate artificial gravity

As mentioned previously, I propose to step up the artificial gravity during the return leg in order to rehabilitate the astronauts to Earth like gravity forces prior to re-entry. I propose that the artificial gravity be slowly, continuously increased day by day over the 996 day return journey so that by the 631^{st} day, with 365 days remaining, the gravity is at 1g. As this is mostly theoretical, with very few experiments of artificial gravity being conducted, I also propose that the condition of the crew members be monitored carefully during the rehabilitation to ensure that any negative effects can be dealt with. The bonus of using liquid hydrogen as the propellant is such that there is a large supply on board (due to it being the main propellant), such that the rate of rehabilitation is flexible throughout the mission, probably the only advantage of a long mission time.

7 Landing

7.1 Landing Site

In order to land on Europa, a suitable landing location must be selected. The environment on Europa means that there are very strict restraints on a suitable landing site, especially for a manned mission. Primarily, Jupiter radiation should be avoided as much as possible therefore the landing site must be on the anti-Jovian hemisphere. Additionally, as Europa's orbital period is ≈85 hours and Jupiter's period of rotation is ≈10, the radiation belt that engulfs Europa is bombarding its trailing hemisphere with ionizing particles. Furthermore, in order for the landing site to be suitable, the landing site must have a low risk during the land, therefore flat, smooth areas are preferred. Finally, the nearby morphology of the surface is of scientific interest.

Combined, the above restrictions leave a very limited choice for a potential landing site. Nevertheless, I have selected a site, as found in, Ivanov et al. (2011), that meets these requirements. An image of the surface location of the primary landing site (E179939R) is seen in Figure 16.

Since the Jupiter facing hemisphere is centered around a longitude of 0°, Grundy et al. (2007), we can see that the selected landing site lies just within the required range to provide ample radiation shielding on surface. Figure 17 shows the image E179939R, Grundy et al. (2007), with the morphological interesting features marked. This landing site is an optimal landing site, not only for its position on the leading, anti-Jovian hemisphere, but also for the geological features. The smooth surface directly where the landing site is (marked by the white arrow in the left hand side image) allows for a larger error in the exact landing site whilst remaining close enough that the crew can perform EVAs (Extravehicular Activities) to interesting geological sites. Additionally, the landing site is found to be relatively flat, which for an icy moon is advantageous as the lander will not slide along the surface when stationary.

Finally, this landing site offers interesting geological features. The smooth surface being near to ridges and fissures suggest that the area is one of cryovolcanic activity. As will be discussed in section 8, samples of the surface material will be taken and should there prove to be cryovolcanic activity in this area then the recycling of the surface will allow for deeper layers of the crust to be analysed. This may give strong scientific evidence towards the sub-surface activity that recycles the surface across the moon. Should there be proof of this recycling of the surface it may also lead to the confirmation that there is liquid water beneath the surface and therefore, should there be a rock-water interface at the core, then there may be potential for life forms, such as organisms, to exist.

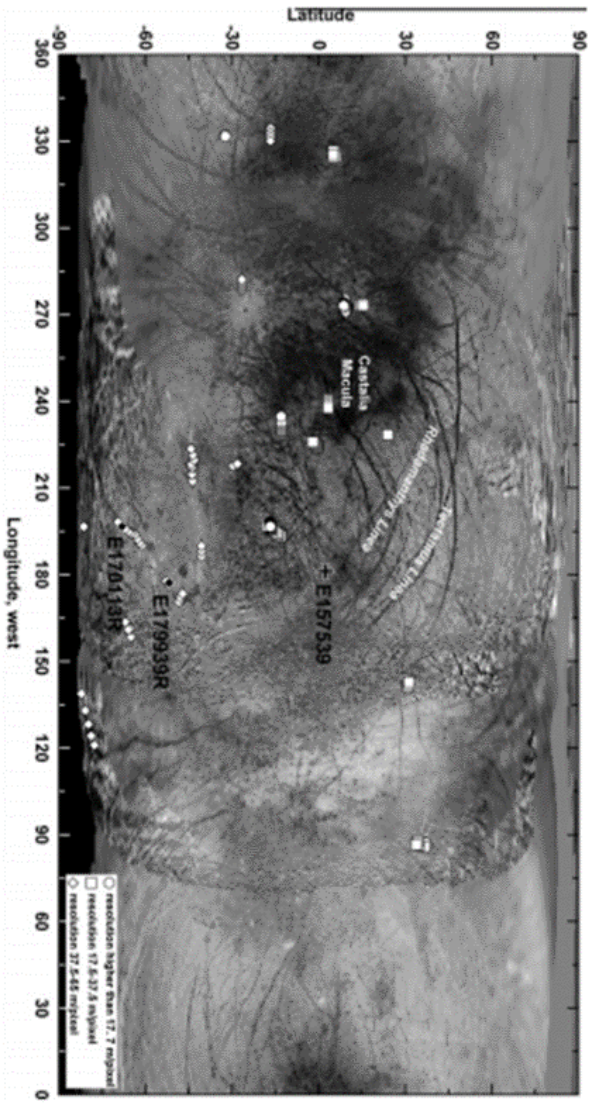

Figure 16: shows the entire surface of Europa with the landing site E179939R marked, courtesy of Ivanov et al. (2011)

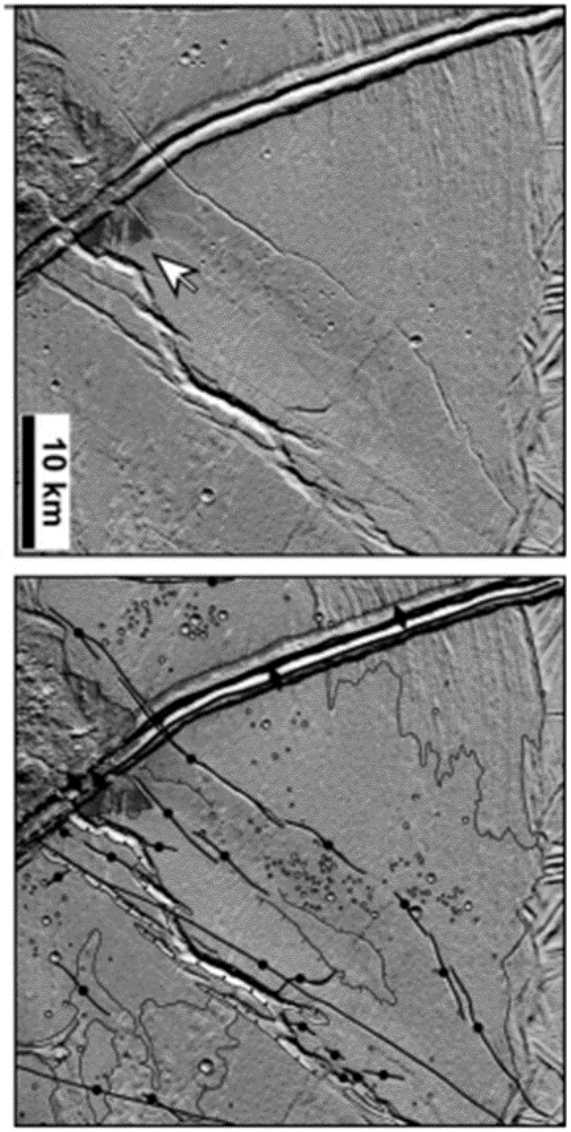

Figure 17: shows the landing site E179939R, **Left** - white arrow indicates landing site, **Right** - indicates the morphologically interesting features, courtesy of Ivanov et al. (2011)

7.2 Landing Method

In order to land on Europa, I propose to use a combination of an airbag system, similar to the method used on the Mars Pathfinder mission, and a landing module, similar to that used in the Apollo missions. As the gravitational field is less, the airbag will not gain as much velocity, therefore a larger mass can be used. The air bag system that was used in the Mars pathfinder mission will therefore be adapted in order to allow for the increased payload mass. The airbags will be the first sequence within the landing, they will contain the supplies, and infrastructure that the astronauts will use whilst inhabiting the moon.

The airbags are made out of a high strength material called Vectran. As discussed in, Hine and Ward, Vectran has a very high modulus, meaning it can undergo large amounts of physical strain without stretching or breaking, making it a good material of choice for an airbag system. The airbag system consists of multiple vented airbags situated beneath the payload mass. Each bag is a crescent shape in order to follow the curves of the payload mass more effectively and has webbing restraints, also of Vectran, around them to add strength to their structure. The main Airbag design is seen in figure 18, with the webbing restraints and the air vent shown.

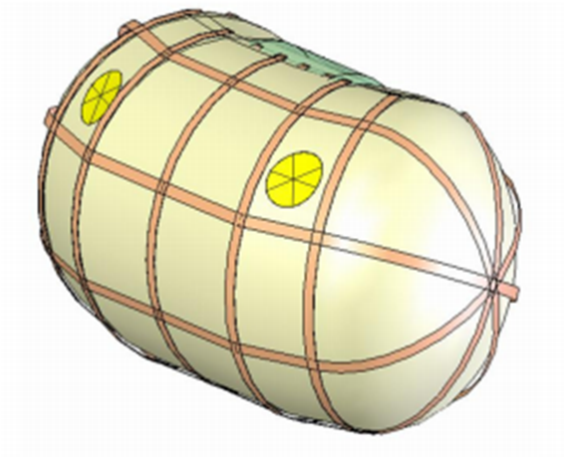

Figure 18: shows the crescent-cylinder shape of the main airbag, with the two release vents in yellow and the webbing restraint design, courtesy of Shook et al. (2009)

The airbag shown in figure 18 is one of six airbags that are in the arrangement as shown in figure 19. The design of the airbag system as described in Shook et al. (2009), is for a Mars landing module with crew on board, as it is designed for a Mars landing it uses parachutes to decelerate to the safe landing velocity. As Europa's atmosphere is extremely tenuous there is insufficient atmosphere to decelerate the module. However, as I am not including the crew in my airbag landing system, the impact velocity can be higher. Due to the lack of atmosphere on Europa, you can occupy an orbit of the moon at extremely low altitudes. The landing system can therefore use a thruster to put the airbag landing system into an orbit that will cause them to land on the surface, without the module gaining too much velocity; 512.8 m/s gained, falling from an orbit of 100 km to the surface. As 512.8 m/s is too fast for the airbag system to survive, the thrusters will be fired a second time at an altitude of 950 m to kill all relative velocity to Europa such that the velocity of impact will be 50 m/s at the surface. The payload mass of each airbag lander is ≈7250 kg, Shook et al. (2009).

The crew landing module will be of a similar design to the Lunar lander module used in the Apollo missions. The only significant changes to the method of landing is that the module must be built to have a far longer lifespan than the lunar module. The altered lander will have a lifespan of over 4750 hours, sufficient to ensure it can launch from Europa's surface to rendezvous

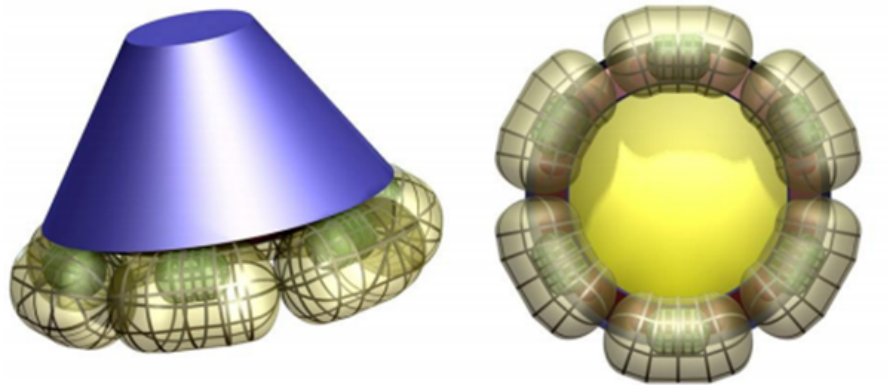

Figure 19: **Left** shows the side on arrangement **Right** shows the arrangement from beneath, Shook et al. (2009)

with the main spacecraft. The Landing module will have a total mass of 15200 kg and will have an engine that can be used for both descent and ascent with a specific impulse of $I_{Spe} = 311$ s^{-1}. The total mass incorporates a payload mass of 2150 kg, the rest attribution to propellant (10840 kg) and the rest the bulk mass of the module. Additionally, payload mass in the launch from Europa's surface has accounted for samples to be returned from the surface.

Finally, by separating the landing stages, the entire of the airbag stage can land before the crew module is released from the main spacecraft. This means that should any problems occur with the airbag landing system, contingencies can be taken before the landing of the human module is initiated.

8 Scientific Goals

In itself, completing a successful mission to the Jovian system and landing humans on another celestial body, outside of Earth's sphere of influence, and returning them safely to Earth will be an incredible scientific feat for humanity. However, on top of this aim there is a lot of interesting science to be done, both in orbit of Europa and on its surface. The following two sections outline just some of the potential goals for the mission.

8.1 Spacecraft Goals

A human mission to the Jovian system offers a lot of exciting new science. Firstly, very little is known about the structure of the radiation belts around Jupiter and the formation of the Io torus. The main spacecraft in my mission proposal will remain in the outer regions of Io's torus for over 4750 hours and that gives 4750 hours of in situ research time. Using spectrometers, such as ROSINA and COSIMA as found used in the Rosetta mission, Glassmeier et al. (2007), the spacecraft can analyse the gas and particles within the torus and the difference of composition to the gas and particles being ejected from Io, giving knowledge to the radiation and ionization processes that can change the gas and particles.

With the spacecraft being in orbit of Jupiter for such a prolonged period, the radiation emission from Jupiter can be studied intensively. The effects this radiation has on the radiation shielding over time can be studied as well as the effects prolonged exposure to the electronics of the spacecraft (although the vital electronics will be shielded). Extensive mapping of Jupiter's surface in high resolution will be achieved across the majority of its surface, monitoring changes within Jupiter's weather system.

8.2 Lander Goals

On the surface of Europa scientific research, that cannot be conducted in orbit, can be carried out during the 4750 hours on the moon. The composition of the surface ice on Europa alone can be studied in intensively, aiding the knowledge of the formation and recycling processes that have formed the lineae, ridges and fissures across the surface, Squyres et al. (1983). The potential for life within the fissures can be studied if there is conclusive evidence that there is a liquid water ocean beneath the icy surface, supplying an environment for their existence. A seismometer placed on the surface would be able to detect the movements of underground oceans, Kovach and Chyba (2001). Further to this, a module that is capable of melting through the ice and surviving under water can be taken to study the liquid ocean below. This module would be highly controversial as should there be a liquid water ocean, life may have developed. Should a module then enter the ocean it may take microbes from Earth with it. This could entirely disrupt a finely balanced ecosystem that could destroy any forms of life that may have developed.

9 Mass Management

I have consolidated the details of all the previous sections in order to calculate the total payload mass of the spacecraft without the inclusion of propellant at the four different stages of the transfers that correspond to the burns. The constituents of the spacecraft at each stage can be seen in Tables 8, 9, 10 and 11.

	Component	Mass (kg)
Heavily Shielded Module	Ammonia Borane Layer	16371
	Ionic Solution	10593
	BNNT Composite	3286
	Lead	7665
Standard Module x 5	BNNT Composite	16430
	Crew (six)	420
Life Support	Reserve Water	1000
	Food	23256
	Oxygen (Air)	1000
	Nitrogen (Air)	2000
Fuel Cells	Oxygen	95363
	Hydrogen	14304
Scientific Equipment	Spacecraft Equipment	2000
	Controls	1000
Landing	Lander module	15200
	Airbag Module	7250
Artificial gravity	Propellant	25882.8496
Earth Escape Mass (LEO)		243020.85

Table 8: shows the constituents of the payload mass at escape from Earth's LEO

	Component	Mass (kg)
Heavily Shielded Module	Ammonia Borane Layer	16371
	Ionic Solution	10593
	BNNT Composite	3286
	Lead	7665
Standard Module x 5	BNNT Composite	16430
	Crew (six)	420
Life Support	Reserve Water	1000
	Food	13953.6
	Oxygen (Air)	1000
	Nitrogen (Air)	2000
Fuel Cells	Oxygen	57217.8
	Hydrogen	8582.4
Scientific Equipment	Spacecraft Equipment	2000
	Controls	1000
Landing	Lander module	15200
	Airbag Module	7250
Artificial gravity	Propellant	19545.081
Europa and Jupiter Capture Mass		183513.881

Table 9: shows the constituents of the payload mass at the time of Jupiter/Europa Capture

	Component	Mass (kg)
Heavily Shielded Module	Ammonia Borane Layer	16371
	Ionic Solution	10593
	BNNT Composite	3286
	Lead	7665
Standard Module x 5	BNNT Composite	16430
	Crew (six)	420
Life Support	Reserve Water	1000
	Food	9302.4
	Oxygen (Air)	1000
	Nitrogen (Air)	2000
Fuel Cells	Oxygen	38145.2
	Hydrogen	5721.6
Scientific Equipment	Spacecraft Equipment	2000
	Controls	1000
Artificial gravity	Propellant	9180.68864
Europa and Jupiter Escape Mass		124114.889

Table 10: shows the constituents of the payload mass at the time of Jupiter/Europa Escape

	Component	Mass (kg)
Heavily Shielded Module	Ammonia Borane Layer	16371
	Ionic Solution	10593
	BNNT Composite	3286
	Lead	7665
Standard Module x 5	BNNT Composite	16430
	Crew (six)	420
Life Support	Reserve Water	1000
	Food	1000
	Oxygen (Air)	1000
	Nitrogen (Air)	2000
Fuel Cells	Oxygen	1907.26
	Hydrogen	286.08
Scientific Equipment	Spacecraft Equipment	2000
	Controls	1000
Artificial gravity	Propellant	3223.56613
Earth Capture Mass		68181.9061

Table 11: shows the constituents of the payload mass at return to Earth LEO

The payload mass at each stage is seen to decrease. This is because of the consumption of the resources throughout the flight. This includes the airbag landing system which will be left on the surface of Europa and therefore not included on the return journey. Additionally, the crew landing module will be jettisoned in orbit of Europa so that its mass is not included in the return transfer. From each of the payload masses, the mass of the propellant required to conduct each of the burns can be calculated, including the fuel required for all burns after that. The mass of fuel required for each burn, in tons, is shown in table 12.

	Burn	Mass (Tons)
Trajectory Burns	Earth capture	186.8364603
	Jupiter Escape	205.6337929
	Europa Escape	190.2690638
	Europa Capture	282.2270073
	Jupiter Capture	693.3655766
	Earth Escape	4936.183085
	Contingency fuel	649.4514986
Total Mass		7143.966485

Table 12: shows the mass of propellant required for each trajectory burn plus the 10% contingency fuel

9.1 Reduction of Mass

Table 12 shows the fuel required for the initial escape burn and the final capture burn are different by a factor of 20. This large difference in mass is due to the extra fuel required to ferry the fuel for later burns, so much so that 96.5% of the mass of the entire mission is purely fuel. Therefore, in order the reduce the mass of fuel required, new methods of propulsion are required to be developed, emphasizing the importance of the developments discussed in section 10. However, considering the payload mass of the spacecraft, I was able to make some reductions to the mass. These were in the form of leaving the airbag landing gear on Europa as well as leaving the lander module in orbit of Europa. Additionally, I reduced the number of modules with radiation shielding to five rather than 23 in order to reduce a significant portion of the mass, giving a total of 24 modules; one heavily shielded, five moderately shielded and 18 non shielded modules. I also considered leaving the heavily shielded module in orbit of Europa, however in the return transfer, the spacecraft will continue to be bombarded by GCRs which will trigger particle showers that require the lead layer to be captured. As a potential solution to this, I considered timing the return transfer to coincide with a solar maximum, therefore reducing the number of GCRs due to the increased strength of the magnetic field within the Heliosphere. However, although this would reduce the thickness of the lead layer required, the solar wind must be taken into account and this still requires to be absorbed through a dense inner layer.

Finally, the current cost of launch from Earth to LEO is ≈£10000 per kg of payload mass. Within this mission proposal a total mass, including fuel, that is required in LEO is ≈7143 tons, this equates to a cost of ≈£71.4 Billion . If interplanetary travel is to become regularly accessible, this cost must be reduced either through the reduction of mass required in LEO or the reduction of launch costs; both of which are discussed in section 10.

10 Prospective Mission Amendments

Throughout the mission proposal I have used the most feasible methods using current and near-future technologies. Within this section I outline a few of the developments which I believe will have significant impacts on the accessibility of interplanetary, human travel.

10.1 Space Colonization

As seen within the Mass Management section 9, one of the largest cost inhibiting factors to interplanetary space travel involves fuel and launch costs. A solution to both of these impediments could be to establish a colony, either in space, on the moon or on another celestial body. For example, if we were to colonize the moon, the moon base could have the capabilities to manufacture radiation shielding, fuel, life support supplies such as air, water and oxygen or even construct entire spacecraft. The compelling advantage of manufacturing resources, parts, or all, of a spacecraft on the moon lies within the smaller gravitational field that it possesses. The result of which means that less propulsion is required to launch spacecraft from the moon therefore reducing the cost of launch per kg to LEO to fractions of the cost compared to the launch from Earth.

Additionally, if asteroid and moon mining further into the solar system were to be considered, as discussed by O'Leary (1988), it would allow for fuel and resources to be acquired throughout the mission therefore reducing the launch mass and reducing the cost of ferrying fuel throughout the mission. Finally, the same can be applied to larger bodies such as Jupiter and Saturn. Within these gas giants lie large amounts of Helium-3, a non-radioactive isotope of Helium that can be used in nuclear fusion reactors. By placing permanent bases in orbit around these gas giants would allow for the harvesting of the fuels they contain. The implications for solar system mining transfer space travel from a purely scientific venture into an economically advantageous venture that will be self sustained creating limitless further opportunities for interplanetary and perhaps interstellar missions, if we can maintain a habitable environment for prolonged periods.

10.2 Experimental Radiation Shielding

The radiation shielding that the proposed mission uses is using traditional methods of element composition and dense materials to absorb the radiation before it enters the spacecraft. These methods are useful and well researched however they attribute a large portion of the mass to the spacecraft and therefore large costs in fuel. There are two types of experimental radiation shielding that within the near future may become the preferred method.

10.2.1 Electrostatic Shielding

One such method is through an electrostatic field that deflects the positively charged particles whilst not attracting the negatively charged plasma. This is accomplished by creating negatively and positively charged nodes external to the spacecraft as shown in figure 20. This attracts and deflects the radiation that would otherwise bombard the spacecraft.

The main advantage of this method of radiation shielding allows the spacecraft to be built of much lighter materials. Tripathi (2011) proposes to use Gossamer structures. Gossamer is fine spider silk that offers high flexibility and extremely low masses that can be stored in very small volumes Jha and Inman (2004). Therefore large structures can be made from Gossamer and stored in small spaces.

The main restriction with the Electrostatic shielding method is the power that is required to maintain a field strong enough field throughout the duration of the mission. This counteracts the mass that is saved in conventional radiation shielding methods. Additionally, Electrostatic radiation shielding has only been tested up to energies of 5keV electrons, Tripathi (2011). As discussed in section 4.2.2 the energies of the surrounding particles of Jupiter are much greater

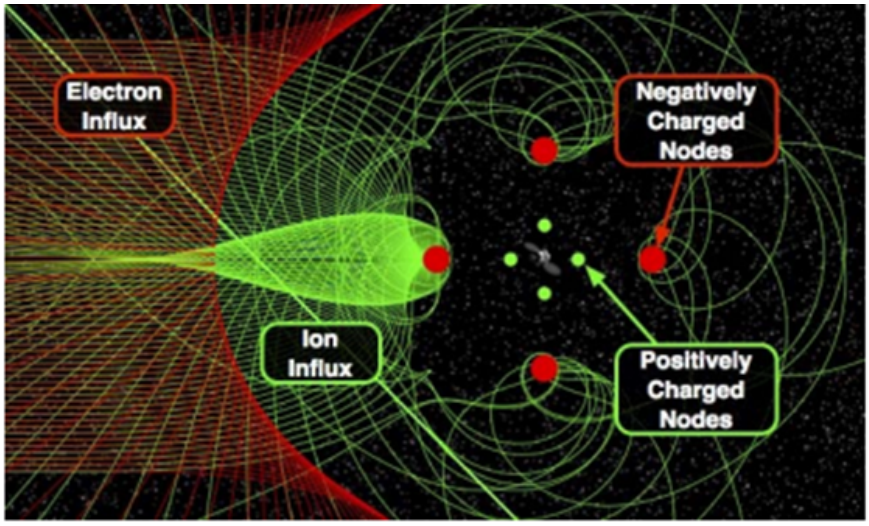

Figure 20: shows the structure of a theoretical Electrostatic method of radiation shielding, courtesy of Tripathi (2011)

than this. We therefore cannot consider this method as feasible until further development has been conducted.

10.2.2 Electromagnetic Shielding

An electromagnetic (EK) radiation shield could be an important step forward for the safety of interplanetary space travel. EM shielding can provide substantial throughout the duration of the mission as well as having capabilities to increase the strength of the magnetic field to protect from high energy coronal mass ejections. An EM shield is generated using a superconducting material in the generator or a solenoid. In order to maintain the low temperatures required by the superconductor a cooling system would also have to be considered, either a closed loop cycle or an open loop cycle using liquid helium or liquid neon to temperatures less than 25k, Kinstler Et. Al. (2009).

The generated magnetic field that embodies the spacecraft acts similar to a magnetosphere of a planet, deflecting the radiation around the spacecraft with some radiation being directed towards the poles, as seen in figure 21. Therefore, moderate shielding of the spacecraft is required at the poles of the magnetic field, however, comparatively to the traditional methods of radiation shielding this is negligible in mass. EM field generators large enough to generate a magnetic field surrounding the entire of the spacecraft will have to produce magnetic fields with strengths between 0.5 and 10 Tesla. For this to be acheived, large generators are required, not only in terms of volume, but also in terms of mass. This somewhat contradicts the saving in the mass of the traditional radiation shielding.

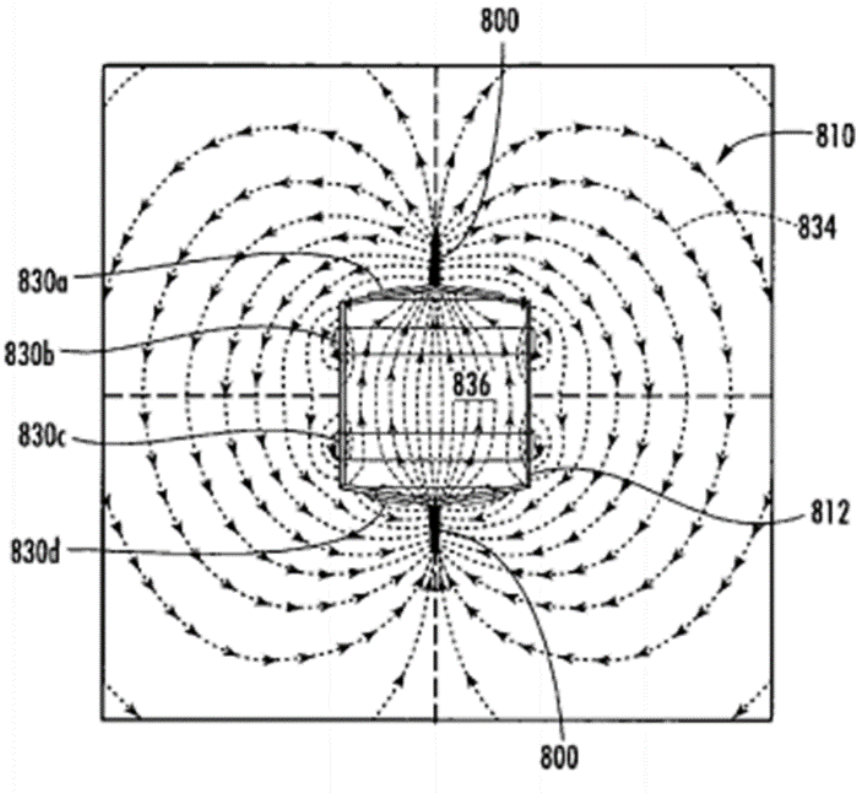

Figure 21: shows the structure of an Electromagnetic method of radiation shielding, courtesy of Kinstler Et. Al. (2009)

10.3 Experimental Propulsion Techniques

10.3.1 Solar Sails

Solar sails are a propulsion method that uses momentum exchange from the photons emitted by the sun to generate momentum transfer. Solar radiation pressure is utilized as the incident photons are reflected off the sail such that a force is generated normal to the sail. Figure 22 shows the fundamental process behind a solar sail. The figure shows a set up for gaining altitude in the orbit as the thrust is in the same direction as the motion of the sail. To decrease orbital energy levels, one would direct the thrust against the direction of motion to decrease kinetic energy and fall into a lower energy orbit. The thrust gained through this method is extremely small, for example, for a 40 m x 40 m square sail at 1AU from the sun the Solar radiation thrust force is $\approx$ 0.03 N, Johnson et al. (2011).

The Japanese space mission, IKAROS, has successfully demonstrated the use of a solar sail of area 196 m^2 (14 m x 14 m) to measure a solar radiation pressure of 1.12 mN at a distance of 1 AU from the sun, Tsuda et al. (2011) and used the solar radiation pressure to descend its orbit around the sun to Venus. Solar sails offer a unique advantage in that they require no fuel. They can therefore perform as many orbital maoeuvres as required; one satellite could theoretically visit all the celestial objects in the solar system, requiring minimal amounts of fuel for alignment corrections. However, the solar radiation pressure is so small, even at 1 AU, that further out in the solar system it will be far smaller as it is inversely proportional to R^2 (the distance from the sun). A consequence of this would be extremely long orbital transfers to outer planets, such as Jupiter. For a human mission this dramatically increases the risks to health due to radiation doses, as discussed in section 5.3. Additionally, Tsuda et al. (2011) found that after unfurling the sail there was a larger than expected amount of torque exerted on the sail which means that

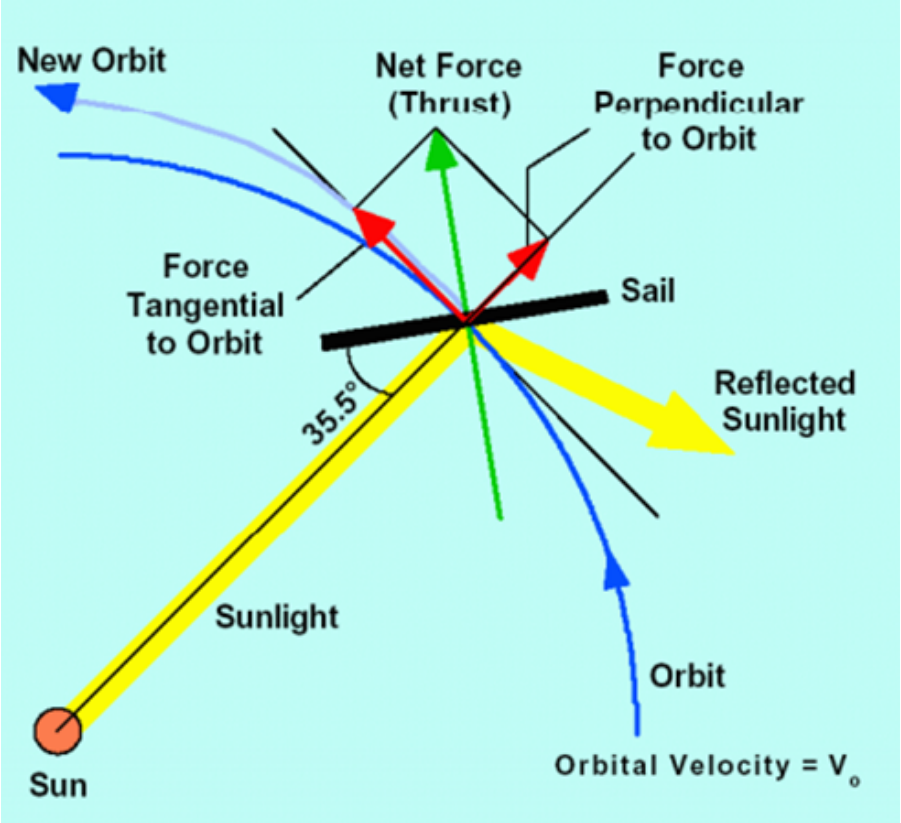

Figure 22: This figure shows the basic schematic for a Solar Sail, courtesy of Johnson et al. (2011)

constant corrections to the yaw, pitch and roll of the spacecraft would be necessary. Furthermore, for a satellite of just 10^{1-2} kg of mass a solar sail of order 10^3 m^2 would be required to give enough thrust force, Johnson et al. (2011).

10.3.2 Electromagnetic Drives

Electromagnetic (EM) drives are a highly controversial and highly theoretical propulsion technique that uses the pressure of microwaves to create a net thrust. The microwave source in an EM drive transfers electrical energy into microwave energy which is transmitted to the resonator cavity, as seen in Figure 23. Thrust is generated by the difference in the group velocity (the speed at which energy of a wave travels) from one end of the truncated cone to the other when the resonator's frequency is equal to that of the wave frequency of the microwaves. The momentum propagating in the cavity is then transferred to the cavity itself, giving the system an overall thrust. The direction of the thrust can be found by taking surface integrals along the cavity surface, Juan Et. Al. (2012).

The controversy developed due to the lack of a propellant such that Newton's third law of motion appears to be broken; there is no conservation of momentum. Despite the skepticism, Juan Et. Al. (2012); Tajmar and Fiedler (2015) have measured a thrust using this method of propulsion. NASA have also confirmed that EM drives work but admit that the thrust is not attributed to any known classical electromagnetic phenomenon. If the theory behind why EM drives work can be properly understood and applied, in more efficient ways than at present, then EM drives may not only be the future of interplanetary travel but may also provide more efficient launches. Shawyer (2015) claims that the future tech of EM Drives can achieve Geostationary orbits with a payload mass of 50 tonnes for a cost a factor of 130 cheaper than current technology.

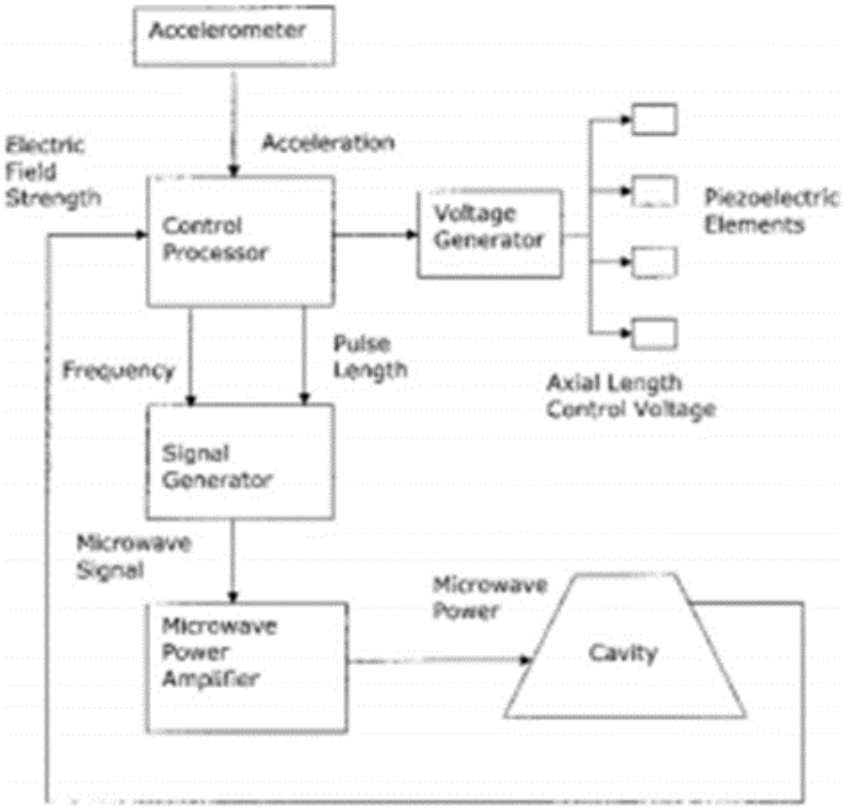

Figure 23: This figure shows the basic schematic for an EM Drive, courtesy of , Shawyer (2015)

Additionally, a ten year mission using EM Drive propulsion could reach velocities up to 0.67c reaching distances of 4 light years, Shawyer (2015) after the ten year propulsion. This technology is expected to be achieved within the next 20 years.

The application of this to interplanetary missions would mean much shorter orbital transfers due to the reduced mass of the spacecraft, because of the lack of propellant. The reduced cost of future missions through the saving of propellant, life support systems and radiation protection may prove that this technology becomes the favoured method.

11 Summary

Throughout the study I have found a suitable target that humans can inhabit for a long duration of time within a safe environment in Europa. I have found that throughout the mission there will be numerous opportunities to further scientific research beyond current achievements. The study found that literature on all topics is easily accessible and can be applied to one's own mission criteria with relative ease. Additionally, section 10 highlights further methods that can be applied to such a mission if one were to dig beneath the surface when searching for an optimum mission plan. The same section also accounts for the improvements that could be made to the project. It offers solutions to the key restrictions in radiation and mass management toward the feasibility of a human mission to the Jovian system and although many are not current technologies, the literature suggests that they will be in the near future.

The fundamentals of this project offer the transferability to any celestial body within the solar system. I believe the method and execution is applicable to any human space mission by changing the parametres involved. If I were to further this study, I would explore the use of gravitational assists using the Oberth effect to optimize my trajectories by using gravity assists in order to reduce the time of the transfer and therefore reduce the dose of radiation for the astronaut. I would also explore the use of asteroids and the Jovian system as a supply for fuel and resources to resupply the spacecraft throughout the mission, therefore saving fuel and mass. As an additional extension to this project, I would conduct a study into the requirements to set up a base on Europa that was capable of re-use such that subsequent missions to the moon would become more cost efficient, both in mass and fuel. This study would also allow for new additions to the base upon each arrival, with the eventual aim of colonizing the moon. I believe that the colonization of Europa is not only feasible but would provide numerous advantages due to the water that is found on Europa, in the form of ice or liquid, combined with the potential for harnessing the Helium-3 within Jupiter to provide supplies and energy for the base. A base on Europa would also aid in future interstellar mission due to being farther from the Sun than Earth making it easier to escape the Sun's gravity.

Overall I believe that the project has been a success, achieving all goals I laid out in my project proposal, surpassing some, i.e. the trajectory simulation was not included in the proposal. I believe that a similar study is more than feasible for a 30 person group of first year undergraduates to conduct over a week. However, in relation to the current mission to Mars programme, I believe the focuses of the groups would have to be re-aligned. This is due to the much larger emphasis on radiation shielding due to the longer exposure times as well as the higher energies of particles surrounding the Jovian system. Furthermore, the Life Support segment of the mission plan benefits from the additional consideration of artificial gravity. Finally, the landing section gains more freedom due to the number of potential candidates within the system. The lower gravity environment of Europa offers a wider selection of landing methods, ranging from landing small probes to an entire spacecraft. Despite this project focuses on a mission to Europa, missions to Ganymede and/or Callisto are also feasible. To conclude, a mission to the Jovian system, in my opinion, is a challenging, rewarding and engaging icebreaker project that is feasible for a group of first year undergraduates to complete.

Bibliography

United Launch Alliance. *Atlas V launch Services User's Guide*. Lockheed Martin, 2010.

Robert M. Bagdigian and Dale Cloud. Status of the international space station regenerative eclss water recovery and oxygen generation systems. 2005. URL http://ntrs.nasa.gov/archive/nasa/casi.ntrs.nasa.gov/20050207456.pdf.

Tom Benson. Liquid rocket engine, 2014. URL https://www.grc.nasa.gov/www/k-12/rocket/lrockth.html.

V. S. Berezinskii, S. V. Bulanov, V. L. Ginzburg, V. A. Dogel, and V. S. Ptuskin. *The astrophysics of cosmic rays*. 1984.

Robert A. Braeunig. Orbital mechanics, 2013. URL http://www.braeunig.us/space/orbmech.htm.

David Brand. Galileo finds jupiter's rings formed by dust blasted off small moons, 1998. URL http://www.news.cornell.edu/stories/1998/09/jupiters-rings-formed-dust-its-satellites.

John R. Brophy. Ion thruster performance model, 1984. URL http://ntrs.nasa.gov/archive/nasa/casi.ntrs.nasa.gov/19850004627.pdf.

Charles D. Brown. Monopropellant systems, 2002. URL http://www.globalspec.com/reference/28350/203279/4-4-monopropellant-systems.

Michael H. Carr Et. Al. Evidence for a subsurface ocean on europa. 1997. URL http://www.nature.com/nature/journal/v391/n6665/abs/391363a0.html.

Layne Carter. Status of the regenerative ecls water recovery system. 2012. URL http://ntrs.nasa.gov/archive/nasa/casi.ntrs.nasa.gov/20100033089.pdf.

U.B. Demirci, S. Bernard, R. Chiriac, F. Toche, and P. Miele. Hydrogen release by thermolysis of ammonia borane {NH3BH3} and then hydrolysis of its by-product [bnhx]. *Journal of Power Sources*, 196(1):279 – 286, 2011. ISSN 0378-7753. doi: http://dx.doi.org/10.1016/j.jpowsour.2010.06.031. URL http://www.sciencedirect.com/science/article/pii/S0378775310010165.

Neil Divine and H. B. Garrett. Charged particle distributions in jupiter's magnetosphere. *Journal of Geophysical Research: Space Physics*, 88(A9):6889–6903, 1983. ISSN 2156-2202. doi: 10.1029/JA088iA09p06889. URL http://dx.doi.org/10.1029/JA088iA09p06889.

Jim Dumoulin. *NSTS 1988 News Reference Manual*. Kennedy Space Center, NASA., 1998.

E. FRIIS-CHRISTENSEN and K. LASSEN. Length of the solar cycle: An indicator of solar activity closely associated with climate. *Science*, 254(5032): 698–700, 1991. ISSN 0036-8075. doi: 10.1126/science.254.5032.698. URL http://science.sciencemag.org/content/254/5032/698.

Karl-Heinz Glassmeier, Hermann Boehnhardt, Detlef Koschny, Ekkehard Kührt, and Ingo Richter. The rosetta mission: Flying towards the origin of the solar system. *Space Science Reviews*, 128(1):1–21, 2007. ISSN 1572-9672. doi: 10.1007/s11214-006-9140-8. URL http://dx.doi.org/10.1007/s11214-006-9140-8.

D. Golberg Et. Al. Boron nitride nanotubes. *Advanced Materials*, 19(18): 2413–2432, 2007. ISSN 1521-4095. doi: 10.1002/adma.200700179. URL http://dx.doi.org/10.1002/adma.200700179.

J. T. Gosling. *Coronal Mass Ejections: An Overview*, pages 9–16. American Geophysical Union, 2013. ISBN 9781118664377. doi: 10.1029/GM099p0009. URL http://dx.doi.org/10.1029/GM099p0009.

Richard Greenberg. Europa, edited by r. t. pappalardo, w. b. mckinnon, and k. khurana. *Meteoritics & Planetary Science*, 46(5):765–766, 2011. ISSN 1945-5100. doi: 10.1111/j.1945-5100.2011.01193.x. URL http://dx.doi.org/10.1111/j.1945-5100.2011.01193.x.

Richard Greenberg, Paul Geissler, Gregory Hoppa, B.Randall Tufts, Daniel D. Durda, Robert Pappalardo, James W. Head, Ronald Greeley, Robert Sullivan, and Michael H. Carr. Tectonic processes on europa: Tidal stresses, mechanical response, and visible features. *Icarus*, 135(1):64 – 78, 1998. ISSN 0019-1035. doi: http://dx.doi.org/10.1006/icar.1998.5986. URL http://www.sciencedirect.com/science/article/pii/S0019103598959863.

W. M. Grundy, B. J. Buratti, A. F. Cheng, J. P. Emery, A. Lunsford, W. B. McKinnon, J. M. Moore, S. F. Newman, C. B. Olkin, D. C. Reuter, P. M. Schenk, J. R. Spencer, S. A. Stern, H. B. Throop, and H. A. Weaver. New horizons mapping of europa and ganymede. *Science*, 318(5848):234–237, 2007. ISSN 0036-8075. doi: 10.1126/science.1147623. URL http://science.sciencemag.org/content/318/5848/234.

Nancy Hall. Solid rocket engine, 2015. URL https://www.grc.nasa.gov/www/k-12/airplane/srockth.html.

J. Hannauer, U. B. Demirci, C. Geantet, J. M. Herrmann, and P. Miele. Enhanced hydrogen release by catalyzed hydrolysis of sodium borohydride-ammonia borane mixtures: a solution-state 11b nmr study. *Phys. Chem. Chem. Phys.*, 13:3809–3818, 2011. doi: 10.1039/C0CP02090G. URL http://dx.doi.org/10.1039/C0CP02090G.

Daniel A. Herman. Nasa's evolutionary xenon thruster (next) project qualification propellant throughput milestone: Performance, erosion and thruster service life prediction after 450kg. 2010. URL http://ntrs.nasa.gov/archive/nasa/casi.ntrs.nasa.gov/20110000521.pdf.

P. J. Hine and I. M. Ward. Measuring the elastic properties of high-modulus fibres. *Journal of Materials Science*, 31(2):371–379. ISSN 1573-4803. doi: 10.1007/BF01139154. URL http://dx.doi.org/10.1007/BF01139154.

M.A. Ivanov, L.M. Prockter, and B. Dalton. Landforms of europa and selection of landing sites. *Advances in Space Research*, 48(4):661 – 677, 2011. ISSN 0273-1177. doi: http://dx.doi.org/10.1016/j.asr.2011.05.016. URL http://www.sciencedirect.com/science/article/pii/S027311771100353X. Europa Lander: Science Goals and Implementation.

Akhilesh K. Jha and Daniel J. Inman. Sliding mode control of a gossamer structure using smart materials. *Journal of Vibration and Control*, 10(8):1199–1220, 2004. doi: 10.1177/1077546304044796. URL http://jvc.sagepub.com/content/10/8/1199.abstract.

Les Johnson, Mark Whorton, Andy Heaton, Robin Pinson, Greg Laue, and Charles Adams. Nanosail-d: A solar sail demonstration mission. *Acta Astronautica*, 68(5–6):571 – 575, 2011. ISSN 0094-5765. doi: http://dx.doi.org/10.1016/j.actaastro.2010.02.008. URL http://www.sciencedirect.com/science/article/pii/S0094576510000597. Special Issue: Aosta 2009 Symposium.

Yang Juan Et. Al. Net thrust measurement of propellantless microwave thruster. *Acta Physica Sinica*, 61(11):110301, 2012. doi: 10.7498/aps.61.110301. URL http://wulixb.iphy.ac.cn/EN/abstract/article_47295.shtml.

K. K. Khurana, M. G. Kivelson, V. M. Vasyliunas, N. Krupp, J. Woch, A. Lagg, B. H. Mauk, and W. S. Kurth. *The configuration of Jupiter's magnetosphere*, pages 593–616. 2004.

Gary A. Kinstler Et. Al. Method and device for magnetic space radiation shield providing isotropic protection, 2009. URL http://www.google.ch/patents/US7484691.

Michelle R. Kirchoff and William B. McKinnon. Formation of mountains on io: Variable volcanism and thermal stresses. *Icarus*, 201(2):598 – 614, 2009. ISSN 0019-1035. doi: http://dx.doi.org/10.1016/j.icarus.2009.02.006. URL http://www.sciencedirect.com/science/article/pii/S0019103509000633.

H. H. Koelle. *Handbook of astronautical engineering.* New York, McGraw-Hill, 1st edition, 1961.

Robert L. Kovach and Christopher F. Chyba. Seismic detectability of a subsurface ocean on europa. *Icarus*, 150(2):279 – 287, 2001. ISSN 0019-1035. doi: http://dx.doi.org/10.1006/icar.2000.6577. URL http://www.sciencedirect.com/science/article/pii/S0019103500965771.

Laboratory for Atmospheric & Space Physics LASP. Magnetosphere of outer planets: Resources. URL http://lasp.colorado.edu/home/science/planetary-science/magnetospheres/resources/.

Kerry Lee. What is space radiation, 2014. URL http://srag-nt.jsc.nasa.gov/spaceradiation/what/what.cfm.

K. Lodders and B. Fegley. *The planetary scientist's companion / Katharina Lodders, Bruce Fegley.* 1998.

Christian Lubich and Alexander Ostermann. Runge-kutta approximation of quasi-linear parabolic equations. *Math. Comp.*, 64:601–627, 1995. URL http://www.ams.org/journals/mcom/1995-64-210/S0025-5718-1995-1284670-0/.

C. S. Mahajan. Mass attenuation coefficients of beta particles in elements. 2012. URL http://www.jsrr.net/Volume%202%20Number%202%20April%2012/CSMahajan21-27.pdf.

NASA. Recycling water and air in space. URL https://www.nasa.gov/pdf/146558main_RecyclingEDA(final)%204_

Jet Propulsion Lab NASA. Planetary satellite discovery circumstances, 2015. URL http://ssd.jpl.nasa.gov/?sat_discovery.

Toxicology Group NASA. Spacecraft maximum allowable concentrations for airbourne contaminants, 1999. URL http://www.cdc.gov/niosh/docket/archive/pdfs/NIOSH-125/125-NASAJSC205841999.pdf.

Brian O'Leary. Asteroid mining and the moons of mars. 17, 1988. URL http://www.sciencedirect.com/science/article/pii/0094576588900598.

Michele Perchonok and Charles Bourland. {NASA} food systems: Past, present, and future. *Nutrition*, 18(10):913 – 920, 2002. ISSN 0899-9007. doi: http://dx.doi.org/10.1016/S0899-9007(02)00910-3. URL http://www.sciencedirect.com/science/article/pii/S0899900702009103.

Robert G. Ragsdale and Edward A. Willis Jr. Gas-core rockets - a new look. 1971. URL http://ntrs.nasa.gov/archive/nasa/casi.ntrs.nasa.gov/19710014431.pdf.

Jon Rask Et. Al. Space faring - the radiation challenge, 2008. URL https://www.nasa.gov/pdf/284273main_Radiation_HS_Mod1.pdf.

W.H. Robbins and H.B. Finger. A historical perspective of the nerva nuclear rocket engine technology program. 1991. URL http://ntrs.nasa.gov/archive/nasa/casi.ntrs.nasa.gov/19910017902.pdf.

Paul M. Schenk and Mark H. Bulmer. Origin of mountains on io by thrust faulting and large-scale mass movements. 279(5356):1514–1517, 1998. ISSN 0036-8075. doi: 10.1126/science.279.5356.1514. URL http://science.sciencemag.org/content/279/5356/1514.

Roger Shawyer. Second generation emdrive propulsion applied to {SSTO} launcher and interstellar probe. *Acta Astronautica*, 116:166 – 174, 2015. ISSN 0094-5765. doi: http://dx.doi.org/10.1016/j.actaastro.2015.07.002. URL http://www.sciencedirect.com/science/article/pii/S0094576515002726.

Dine E. Sherif and James C. Knox. International space station carbon dioxide removal assembly (iss cdra) concepts and advancements, 2005. URL http://ntrs.nasa.gov/archive/nasa/casi.ntrs.nasa.gov/20050210002.pdf.

Lauren S. Shook, Richard B. Timmers, and Jon Hinkle. Second generation airbag landing system for the orion crew module. 2009. URL http://enu.kz/repository/2009/AIAA-2009-2989.pdf.

Adam P. Showman and Renu Malhotra. The galilean satellites. *Science*, 286 (5437):77–84, 1999. ISSN 0036-8075. doi: 10.1126/science.286.5437.77. URL http://science.sciencemag.org/content/286/5437/77.

Damon P. Simonelli, Laura Rossier, Peter C. Thomas, Joseph Veverka, Joseph A. Burns, and Michael J.S. Belton. Leading/trailing albedo asymmetries of thebe, amalthea, and metis. *Icarus*, 147(2):353 – 365, 2000. ISSN 0019-1035. doi: http://dx.doi.org/10.1006/icar.2000.6474. URL http://www.sciencedirect.com/science/article/pii/S0019103500964741.

SpaceX. *Falcon 9 Launch Vehicle Payload user's guide*. Space Exploration Technologies corporation, 2009.

John R. Spencer, Leslie K. Tamppari, Terry Z. Martin, and Larry D. Travis. Temperatures on europa from galileo photopolarimeter-radiometer: Nighttime thermal anomalies. *Science*, 284(5419):1514–1516, 1999. ISSN 0036-8075. doi: 10.1126/science.284.5419.1514. URL http://science.sciencemag.org/content/284/5419/1514.

S. W. Squyres, R. T. Reynolds, and P. M. Cassen. Liquid water and active resurfacing on Europa. *nat*, 301:225, January 1983. doi: 10.1038/301225a0.

E. C. STONE and A. L. LANE. Voyager 1 encounter with the jovian system. *Science*, 204(4396):945–948, 1979. ISSN 0036-8075. doi: 10.1126/science.204.4396.945. URL http://science.sciencemag.org/content/204/4396/945.

M. Tajmar and G. Fiedler. Direct thrust measurements of an em drive and evaluation of possible side-effects. 2015. URL http://dx.doi.org/10.2514/6.2015-4083.

P.C. Thomas, J.A. Burns, L. Rossier, D. Simonelli, J. Veverka, C.R. Chapman, K. Klaasen, T.V. Johnson, and M.J.S. Belton. The small inner satellites of jupiter. *Icarus*, 135(1): 360 – 371, 1998. ISSN 0019-1035. doi: http://dx.doi.org/10.1006/icar.1998.5976. URL http://www.sciencedirect.com/science/article/pii/S0019103598959760.

Lawrence W. Townsend. Implications of the space radiation environment for human exploration in deep space. *Radiation Protection Dosimetry*, 115(1-4):44–50, 2005. doi: 10.1093/rpd/nci141. URL http://rpd.oxfordjournals.org/content/115/1-4/44.abstract.

Ram K. Tripathi. Meeting the grand challenge of protecting astronaut's health: Electrostatic active space radiation shielding for deep space missions. 2011. URL https://www.nasa.gov/pdf/718390main_Tripathi_2011_PhI_Electrostatic_Radiation_Protection.pdf.

Y. Tsuda, O. Mori, R. Funase, H. Sawada, T. Yamamoto, T. Saiki, T. Endo, and J. Kawaguchi. Flight status of {IKAROS} deep space solar sail demonstrator. *Acta Astronautica*, 69(9–10): 833 – 840, 2011. ISSN 0094-5765. doi: http://dx.doi.org/10.1016/j.actaastro.2011.06.005. URL http://www.sciencedirect.com/science/article/pii/S0094576511001822.

James E. Turner. *Atoms, Radiation and Radiation Protection*, volume 3. Wiley-VCH, 2007.

Jonathon L. Van Noord. Lifetime assessment of the next ion thruster. 2007. URL https://www.grc.nasa.gov/WWW/ion/pdfdocs/AIAA-2007-5274.pdf.

M. Warshay, P. Prokopius, M. Le, and G. Voecks. The nasa fuel cell upgrade program for the space shuttle orbiter. In *Energy Conversion Engineering Conference, 1997. IECEC-97., Proceedings of the 32nd Intersociety*, volume 1, pages 228–231 vol.1, Jul 1997. doi: 10.1109/IECEC.1997.659189.

Roy Whitney. Advanced shielding for astronauts and equipment. 2016.

Dr. D. R. Williams. Trajectories and orbits. URL http://history.nasa.gov/conghand/traject.htm.

Dr. D. R. Williams. Earth fact sheet, 2016. URL http://nssdc.gsfc.nasa.gov/planetary/factsheet/earthfact.html.

David E. Williams Et. Al. International space station environment control and life supoort systems status for the prior year: 2012-2011. 2011. URL http://ntrs.nasa.gov/archive/nasa/casi.ntrs.nasa.gov/20120012940.pdf.

L. R. Young. Artificial Gravity Considerations for a Mars Exploration Mission. *Annals of the New York Academy of Sciences*, 871:367–378, May 1999. doi: 10.1111/j.1749-6632.1999.tb09198.x.

Appendices

A Tables

A.1 The Jovian System

Table 13: shows the 67 Jovian satellites, sourced from , NASA (2015)

Satellites of Jupiter: 67					
IAU number	**IAU name**	**Provisional designation**	**Year discovered**	**Discoverer(s)/Spacecraft mission**	**References**
I	Io		1610	Galileo	
II	Europa		1610	Galileo	
III	Ganymede		1610	Galileo	
IV	Callisto		1610	Galileo	
V	Amalthea		1892	E.E. Barnard	
VI	Himalia		1904	C. Perrine	
VII	Elara		1905	C. Perrine	
VIII	Pasiphae		1908	P. Melotte	
IX	Sinope		1914	S.B. Nicholson	
X	Lysithea		1938	S.B. Nicholson	
XI	Carme		1938	S.B. Nicholson	
XII	Ananke		1951	S.B. Nicholson	
XIII	Leda		1974	C. Kowal	
XIV	Thebe	S/1979 J2	1980	Voyager Science Team	
XV	Adrastea	S/1979 J1	1979	Voyager Science Team	
XVI	Metis	S/1979 J3	1980	Voyager Science Team	
XVII	Callirrhoe	S/1999 J1	1999	J.V. Scotti, T.B. Spahr, R.S. McMillan, J.A. Larsen, J. Montani, A.E. Gleason, T. Gehrels	IAUC 7460
XVIII	Themisto	S/1975 J1 S/2000 J1	2000	S.S. Sheppard, D.C. Jewitt, Y. Fernandez, G. Magnier	IAUC 7525
XIX	Megaclite	S/2000 J8	2000	S.S. Sheppard, D.C. Jewitt, Y. Fernandez, G. Magnier	IAUC 7555
XX	Taygete	S/2000 J9	2000	S.S. Sheppard, D.C. Jewitt, Y. Fernandez, G. Magnier	IAUC 7555
XXI	Chaldene	S/2000 J10	2000	S.S. Sheppard, D.C. Jewitt, Y. Fernandez, G. Magnier	IAUC 7555
XXII	Harpalyke	S/2000 J5	2000	S.S. Sheppard, D.C. Jewitt, Y. Fernandez, G. Magnier	IAUC 7555
XXIII	Kalyke	S/2000 J2	2000	S.S. Sheppard, D.C. Jewitt, Y. Fernandez, G. Magnier	IAUC 7555
XXIV	Iocaste	S/2000 J3	2000	S.S. Sheppard, D.C. Jewitt, Y. Fernandez, G. Magnier	IAUC 7555
XXV	Erinome	S/2000 J4	2000	S.S. Sheppard, D.C. Jewitt, Y. Fernandez, G. Magnier	IAUC 7555
XXVI	Isonoe	S/2000 J6	2000	S.S. Sheppard, D.C. Jewitt, Y. Fernandez, G. Magnier	IAUC 7555
XXVII	Praxidike	S/2000 J7	2000	S.S. Sheppard, D.C. Jewitt, Y. Fernandez, G. Magnier	IAUC 7555
XXVIII	Autonoe	S/2001 J1	2001	S.S. Sheppard, D.C. Jewitt, J. Kleyna	MPEC 2002-J54
XXIX	Thyone	S/2001 J2	2001	S.S. Sheppard, D.C. Jewitt, J. Kleyna	MPEC 2002-J54
XXX	Hermippe	S/2001 J3	2001	S.S. Sheppard, D.C. Jewitt, J. Kleyna	MPEC 2002-J54
XXXI	Aitne	S/2001 J11	2001	S.S. Sheppard, D.C. Jewitt, J. Kleyna	MPEC 2002-J54
XXXII	Eurydome	S/2001 J4	2001	S.S. Sheppard, D.C. Jewitt, J. Kleyna	MPEC 2002-J54
XXXIII	Euanthe	S/2001 J7	2001	S.S. Sheppard, D.C. Jewitt, J. Kleyna	MPEC 2002-J54

XXXIV	Euporie	S/2001 J10	2001	S.S. Sheppard, D.C. Jewitt, J. Kleyna	MPEC 2002-J54
XXXV	Orthosie	S/2001 J9	2001	S.S. Sheppard, D.C. Jewitt, J. Kleyna	MPEC 2002-J54
XXXVI	Sponde	S/2001 J5	2001	S.S. Sheppard, D.C. Jewitt, J. Kleyna	MPEC 2002-J54
XXXVII	Kale	S/2001 J8	2001	S.S. Sheppard, D.C. Jewitt, J. Kleyna	MPEC 2002-J54
XXXVIII	Pasithee	S/2001 J6	2001	S.S. Sheppard, D.C. Jewitt, J. Kleyna	MPEC 2002-J54
XXXIX	Hegemone	S/2003 J8	2003	S.S. Sheppard	IAUC 8088
XL	Mneme	S/2003 J21	2003	S.S. Sheppard, B. Gladman	IAUC 8138
XLI	Aoede	S/2003 J7	2003	S.S. Sheppard	IAUC 8087
XLII	Thelxinoe	S/2003 J22	2003	S.S. Sheppard, B. Gladman	IAUC 8276
XLIII	Arche	S/2002 J1	2003	S.S. Sheppard	IAUC 8035
XLIV	Kallichore	S/2003 J11	2003	S.S. Sheppard	IAUC 8089
XLV	Helike	S/2003 J6	2003	S.S. Sheppard	IAUC 8087
XLVI	Carpo	S/2003 J20	2003	S.S. Sheppard	IAUC 8125
XLVII	Eukelade	S/2003 J1	2003	S.S. Sheppard	IAUC 8087
XLVIII	Cyllene	S/2003 J13	2003	S.S. Sheppard	IAUC 8116
XLIX	Kore	S/2003 J14	2003	S.S. Sheppard	IAUC 8116
L	Herse	S/2003 J17	2003	B. Gladman	IAUC 8116
LI		S/2010 J1	2010	R. Jacobson, M. Brozovic, et al.	IAUC 9222
LII		S/2010 J2	2010	C. Veillet	IAUC 9222
LIII	Dia	S/2000 J11	2000	S.S. Sheppard, D.C. Jewitt, Y. Fernandez, G. Magnier	IAUC 7555
		S/2003 J2	2003	S.S. Sheppard	IAUC 8087
		S/2003 J3	2003	S.S. Sheppard	IAUC 8087
		S/2003 J4	2003	S.S. Sheppard	IAUC 8087
		S/2003 J5	2003	S.S. Sheppard	IAUC 8087
		S/2003 J9	2003	S.S. Sheppard	IAUC 8089
		S/2003 J10	2003	S.S. Sheppard	IAUC 8089
		S/2003 J12	2003	S.S. Sheppard	IAUC 8089
		S/2003 J15	2003	S.S. Sheppard	IAUC 8116
		S/2003 J16	2003	B. Gladman	IAUC 8116
		S/2003 J18	2003	B. Gladman	IAUC 8116
		S/2003 J19	2003	B. Gladman	IAUC 8125
		S/2003 J23	2003	S.S. Sheppard	IAUC 8281
		S/2011 J1	2011	S.S. Sheppard	CBET 3002/IAUC 9252
		S/2011 J2	2011	S.S. Sheppard	CBET 3002/IAUC 9252

A.2 Liquid Fuel Engines

Table 14: This table shows the different types of Monopropellant fuel available, courtesy of , Koelle (1961)

Chemical	Density	Flame temperature, K	I_{sp}, s	Sensitivity
Methyl nitrate	1.21	3716	259	Yes
Nitromethane	1.13	2479	244	Yes
Nitroglycerine	1.60	3309	244	Yes
Ethyl nitrate	1.10	1944	224	Yes
Hydrazine	1.01	1394	230	No
Tetronitromethane	1.65	2170	180	Yes
Hydrogen peroxide	1.45	1277	165	No
Ethylene oxide	0.87	1233	189	No
n-Propyl nitrate	1.06	1693	201	Yes

B Code

B.1 Main Code

```
clear all;
close all;
clc;

G = 6.67*10^-11;                                    %Gravitational Constant
DelV_initial = 6306.5;                              %Initial Burn DelV

%Masses of bodies

m_Earth = 5.972*10^24;        %Earth mass
m_Sun = 1.989*10^30;          %Sun mass
m_Jupiter = 1.898*10^27;      %Jupiter mass
m_spce = 100000;              %Spacecraft mass

%Normalising mass

Mnorm = m_Earth + m_spce;

%Normalized Masses

mu_E = m_Earth/Mnorm;         %Normilized Earth Mass
mu_S = m_Sun/Mnorm;           %Normilized Sun mass
mu_J = m_Jupiter/Mnorm;       %Normilized Jupiter mass
mu_spce = m_spce/Mnorm;       %Normilized Spacecraft mass

%Orbital radius of bodies

r_Eur = 670900000+69911000; %Europa orbital radius
r_spce = 6371000+160000;    %Spacecraft orbital radius
r_Earth = 149.59787*10^9;   %Earth orbital radius
r_Jupiter = 778*10^9;       %Jupiter orbital radius

%Normilizing length unit

a = r_spce;                 %Normilizing length unit

%Normilized radii

rd_Eur = r_Eur/a;           %Normilized Europa orbital radius
rd_E = r_Earth/a;           %Normilized Earth orbital radius
rd_J = r_Jupiter/a;         %Normilized Jupiter orbital radius
rd_spce = r_spce/a;         %Normilized Spacecraft orbital radius

%Normalized Initial DeltaV

DelVd_initial = DelV_initial/sqrt(G*Mnorm/a);

%Alignment Angles

alpha = 2.681;      %Launch Alignment
beta = 0.456988;    %Hyperbolic Escape Alignment

```

Figure 24: This code shows the main code of the Hohmann transfer simulation (page 1/4)

```
52
53      %Initial Conditions
54
55 -    x0_spce = rd_E + rd_spce*cos(beta);                                          %Speacecraft initial x position
56 -    y0_spce = -rd_spce*sin(beta);                                                %Spacecraft initial y position
57 -    vx0_spce = -sqrt(mu_E)*sin(-beta)-DelVd_initial*sin(-beta);                  %Spacecraft initial x velocity
58 -    vy0_spce = sqrt(mu_S/rd_E)+sqrt(mu_E)*cos(-beta)+DelVd_initial*cos(-beta);   %Spacecraft initial y velocity
59 -    x0_E = rd_E;                                                                 %Earth initial x position
60 -    y0_E = 0;                                                                    %Earth initial y position
61 -    vx0_E = 0;                                                                   %Earth initial x velocity
62 -    vy0_E = sqrt(mu_S/rd_E)-sqrt(mu_spce);                                       %Earth initial y velocity
63 -    vx0_J = -sqrt(mu_S/rd_J)*sin(3*pi/2-alpha);                                  %Jupiter initial x velocity
64 -    vy0_J = sqrt(mu_S/rd_J)*cos(3*pi/2-alpha);                                   %Jupiter initial y velocity
65 -    x0_J = rd_J*cos(3*pi/2-alpha);                                               %Jupiter initial x position
66 -    y0_J = rd_J*sin(3*pi/2-alpha);                                               %Jupiter initial y position
67 -    X_spce = [x0_spce,y0_spce,vx0_spce,vy0_spce,x0_E,y0_E,vx0_E,vy0_E,x0_J,y0_J,vx0_J,vy0_J];   %Initial conditions array
68
69      %For loop parameters
70
71 -    b = 0;                                  %initial time
72 -    c = 86081401.9/(sqrt(a^3/(G*Mnorm)));   %Transfer time
73 -    h = 0.1;                                %Iteration time step
74 -    t = b:h:c-h;                            %time array
75 -    N = (c-b)/h;                            %Number of steps
76
77      %Loop iterates positions and velocities until encounter
78
79 -    for i = 1:N
80 -        XArray_spce(:,i) = X_spce;                                %Adds iteration to Xarray
81 -        Comoving(1,i) = X_spce(5)-X_spce(1);                      %Following 4 lines calculate co-moving coordinates
82 -        Comoving(2,i) = X_spce(6)-X_spce(2);
83 -        Comoving(3,i) = X_spce(9)-X_spce(1);
84 -        Comoving(4,i) = X_spce(10)-X_spce(2);
85 -        X_spce = RungeEspceTest(h,X_spce,mu_E,mu_spce,mu_S,mu_J);   %Iterates Array by calling function RungEspceTest(X)
86 -    end
87
88      %Secondary burn and normilized
89
90 -    DelV_Secondary = 6143.59485;                        %Secondary burn DelV
91 -    DelVd_secondary = DelV_Secondary/sqrt(G*Mnorm/a);   %Normilized secondary burn
92
93      %Following lines give new initial conditions of spacecraft after secondary
94      %Burn (In Jupiter f.o.r.)
95
96 -    R_Jspce = sqrt((X_spce(1)-X_spce(9))^2+(X_spce(2)-X_spce(10))^2);
97 -    vel = sqrt(mu_J/R_Jspce);
98 -    velact = sqrt((X_spce(3)-X_spce(11))^2+(X_spce(4)+X_spce(12))^2);
99 -    angleJ = atan(X_spce(12)/X_spce(11));
100 -   angleSp = atan(X_spce(4)/X_spce(3));
101
102 -   v_delexc = DelVd_secondary - (X_spce(11)-X_spce(3) + X_spce(12)-X_spce(4));
103 -   velmag = sqrt((vel*sin(3*pi/2+angleJ))^2+(vel*cos(3*pi/2+angleJ))^2);
```

Figure 25: This code shows the main code of the Hohmann transfer simulation (page 2/4)

```
104
105     %Redefines X array
106
107 -   X = X_spce;
108
109     %Sets periapsis of orbit
110
111 -   R_p = rd_Eur;
112
113     %Sets intitial distance from Jupiter
114
115 -   R_0 = sqrt((X(1)-X(9))^2+(X(2)-X(10))^2);
116
117     %Sets initial Angle to Jupiter
118
119 -   f_0 = atan(X(2)/X(1));
120 -   tau_0 = (R_p)^(3/2)*sqrt(2)/3*tan(-f_0/2)*(3+tan(-f_0/2)^2);
121
122     %New Initial Conditions
123
124 -   x_p = X(1)-X(9);                                    %Initial spacecraft x position
125 -   y_p = X(2)-X(10);                                   %initial spaceraft y position
126 -   x_s = 0;                                            %Initial Jupiter x position
127 -   y_s = 0;                                            %Initial Jupiter y position
128 -   v_px = sqrt(mu_J/R_0)*sin(f_0);                     %Initial spacecraft x velocity
129 -   v_py = -sqrt(mu_J/R_0)*cos(f_0);                    %Initial spacecraft y velocity
130 -   v_sx = 0;                                           %initial Jupiter x velocity
131 -   v_sy = 0;                                           %Initial Jupiter y velocity
132 -   X_J = [x_p,y_p,v_px,v_py,x_s,y_s,v_sx,v_sy];
133
134     %New Parameters
135
136 -   b = 0;                              %initial time
137 -   c = 20;                             %Transfer time
138 -   h = 0.1;                            %Iteration time step
139 -   t = b:h:c-h;                        %time array
140 -   N = (c-b)/h;                        %Number of steps
141
142     %Iterates for the new array
143
144 -   for i = 1:N
145 -       XArrayJ(:,i) = X_J;
146 -       ComovingJ(1,i) = X_J(5)-X_J(1);
147 -       ComovingJ(2,i) = X_J(6)-X_J(2);
148 -       X_J = RungeJ(h,X_J,mu_J,mu_spce);
149 -   end
150
151     %Aligns Capture trajectory to Sun f.o.r.
152
153 -   XArrayJnew(1,:) = XArrayJ(1,:) + X_spce(9);
154 -   XArrayJnew(2,:) = XArrayJ(2,:) + X_spce(10);
155
```

Figure 26: This code shows the main code of the Hohmann transfer simulation (page 3/4)

```
155
156     %Hereafter plots graphs
157
158 -   figure('Name','Numerical Star System','NumberTitle','off')
159 -   plot(XArray_spce(9,:),XArray_spce(10,:),'k:')
160 -   hold on
161 -   plot(XArray_spce(1,:),XArray_spce(2,:),'r-')
162 -   hold on
163 -   plot(XArray_spce(5,:),XArray_spce(6,:),'b:')
164 -   hold on
165 -   plot(XArray_spce(9,1),XArray_spce(10,1),'kx')
166 -   hold on
167 -   plot(XArray_spce(1,1),XArray_spce(2,1),'rx')
168 -   hold on
169 -   plot(XArray_spce(5,1),XArray_spce(6,1),'bx')
170 -   hold on
171 -   plot(XArrayJnew(1,:),XArrayJnew(2,:),'r-')
172 -   xlabel('Dimensionless x position [a]')
173 -   ylabel('Dimensionless y position [a]')
174 -   legend('Jupiter Orbit','Spacecraft Transfer Orbit','Earth orbit','Jupiter initial Position','Spacecraft Initial Position','Earth initial Position', 'location', 'northeast')
175 -   axis equal;
176
177 -   figure('Name','Numerical Binary Star Comoving position earth','NumberTitle','off')
178 -   plot(Comoving(1,:), Comoving(2,:),'k-')
179 -   hold on
180 -   plot(ComovingJ(1,:), ComovingJ(2,:),'b-')
181 -   hold on
182 -   xlabel('Comoving x Position [a]')
183 -   ylabel('Comoving y Position [a]')
184 -   axis equal
185
186 -   figure('Name','Numerical Binary Star Comoving position Jupiter','NumberTitle','off')
187 -   plot(-Comoving(3,:), -Comoving(4,:),'g-')
188 -   hold on
189 -   plot(XArrayJ(1,:), -XArrayJ(2,:),'r-')
190 -   hold on
191 -   plot(0,0,'bx')
192 -   xlabel('Comoving x Position [a]')
193 -   ylabel('Comoving y Position [a]')
194 -   axis equal
195
196 -   figure('Name','Numerical spacecraft velocity','NumberTitle','off')
197 -   plot(XArray_spce(3,:),XArray_spce(4,:),'r-')
198 -   hold on
199 -   plot(XArray_spce(3,:),XArray_spce(4,:),'b-')
200 -   xlabel('Comoving x Position [a]')
201 -   ylabel('Comoving y Position [a]')
202 -   axis equal
203
```

Figure 27: This code shows the main code of the Hohmann transfer simulation (page 4/4)

B.2 Functions

```
function Xnew = RungeEspceTest(h,X,m_s,m_p,M,mu_J)
    k_1 = h*EspceTest(X,m_s,m_p,M,mu_J);          %Calls upon function EspceTest(X) to calculate the k_1
    k_2 = h*EspceTest(X+k_1/2,m_s,m_p,M,mu_J);
    k_3 = h*EspceTest(X+k_2/2,m_s,m_p,M,mu_J);
    k_4 = h*EspceTest(X+k_3,m_s,m_p,M,mu_J);
    Xnew = X + k_1/6+k_2/3+k_3/3+k_4/6;           %Combines the four steps in the Runge-Kutta Approximation formula
```

Figure 28: This code shows the RungeEspceTest function as called upon in the main code

```
function output = EspceTest(X,m_s,m_p,M,mu_J)
r = sqrt((X(1)-X(5))^2+(X(2)-X(6))^2);              %Calculates Spacecraft-Earth distance
R_p = sqrt(X(1)^2+X(2)^2);                          %Calculates Spacecraft-Sun distance
R_s = sqrt(X(5)^2+X(6)^2);                          %Calculates Earth-Sun distance
r_pJ = sqrt((X(1)-X(9))^2+(X(2)+X(10))^2);          %Calculates Spacecraft-Jupiter Distance
R_JS = sqrt(X(9)^2+X(10)^2);                        %Calculates Jupiter-Sun distance
output(1) = X(3);
output(2) = X(4);
output(3) = (mu_J/r_pJ^3)*(X(9)-X(1))+(m_s/r^3)*(X(5)-X(1))-(M/R_p^3)*X(1);   %Equation of motion primary x
output(4) = (mu_J/r_pJ^3)*(X(10)-X(2))+(m_s/r^3)*(X(6)-X(2))-(M/R_p^3)*X(2);  %Equation of motion primary y
output(5) = X(7);
output(6) = X(8);
output(7) = -(M/R_s^3)*X(5);   %Equation of motion secondary x
output(8) = -(M/R_s^3)*X(6);   %Equation of motion secondary y
output(9) = X(11);
output(10) = X(12);
output(11) = -(M/R_JS^3)*X(9);
output(12) = -(M/R_JS^3)*X(10);
```

Figure 29: This code shows the EspceTest function as called upon in the main code

```
function Xnew = RungeJ(h,X,m_s,m_p)
    k_1 = h*J(X,m_s,m_p);
    k_2 = h*J(X+k_1/2,m_s,m_p);
    k_3 = h*J(X+k_2/2,m_s,m_p);
    k_4 = h*J(X+k_3,m_s,m_p);
    Xnew = X + k_1/6+k_2/3+k_3/3+k_4/6;
```

Figure 30: This code shows the RungeJ function as called upon in the main code

```
function output = J(X,m_s,m_p)
r = sqrt((X(1)-X(5))^2+(X(2)-X(6))^2);
output(1) = X(3);
output(2) = X(4);
output(3) = (m_s/r^3)*(X(5)-X(1));   %Equation of motion primary x
output(4) = (m_s/r^3)*(X(6)-X(2));   %Equation of motion primary y
output(5) = X(7);
output(6) = X(8);
output(7) = (m_p/r^3)*(X(1)-X(5));   %Equation of motion secondary x
output(8) = (m_p/r^3)*(X(2)-X(6));   %Equation of motion secondary y
```

Figure 31: This code shows the J function as called upon in the main code

C Derivations

C.1 Vis-Viva Equation

On a closed orbit, specific total energy is constant and is constructed of the kinetic energy and the gravitational potential energy of the object. In the following derivation, I have assumed the mass of the orbiting body to be negligible, i.e. the central mass $M >> m$:

$$\epsilon = \frac{v_a^2}{2} - \frac{GM}{r_a} = \frac{v_p^2}{2} - \frac{GM}{r_p} \tag{37}$$

Where ϵ is specific total energy, a subscript a denotes apoapsis, subscript p denotes periapse, M denotes the mass of the Sun, G is the gravitational constant.

Rearranging:

$$\frac{v_a^2}{2} - \frac{v_p^2}{2} = \frac{GM}{r_a} - \frac{GM}{r_p} \tag{38}$$

Using the conservation of angular momentum:

$$h = r_p v_p = r_a v_a \tag{39}$$

Rearranging:

$$v_p = \frac{r_a}{r_p} v_a \tag{40}$$

Therefore:

$$\frac{1}{2}\left(1 - \frac{r_a^2}{r_p^2}\right) v_a^2 = \frac{GM}{r_a} - \frac{GM}{r_p} \tag{41}$$

$$\frac{1}{2}\left(\frac{r_p^2 - r_a^2}{r_p^2}\right) v_a^2 = \frac{GM}{r_a} - \frac{GM}{r_p} \tag{42}$$

$$\frac{1}{2} v_a^2 = GM\left(\frac{1}{r_a} - \frac{1}{r_p}\right)\left(\frac{r_p^2}{r_p^2 - r_a^2}\right) = GM\frac{r_p}{r_a\left(r_p + r_a\right)} \tag{43}$$

Using the definition for the semimajor axis:

$$2a = r_a + r_p \tag{44}$$

$$\frac{1}{2} v_a^2 = GM\frac{2a - r_a}{r_a\left(2a\right)} \tag{45}$$

Subbing into the specific total energy equation:

$$\epsilon = \frac{v_a^2}{2} - \frac{GM}{r_a} \tag{46}$$

Becomes:

$$\epsilon = GM\frac{2a - r_a}{2a r_a} - \frac{GM}{r_a} \tag{47}$$

$$\epsilon = GM\left(\frac{2a - r_a}{2a r_a} - \frac{1}{r_a}\right) \tag{48}$$

$$\epsilon = -\frac{GM}{2a} \tag{49}$$

Rewriting the specific total energy:

$$-\frac{GM}{2a} = \frac{v^2}{2} - \frac{GM}{r} \tag{50}$$

To give:

$$v^2 = GM\left(\frac{2}{r} - \frac{1}{a}\right) \tag{51}$$

C.2 Hohmann Transfer

To derive the Hohmann transfer burns we start from the Vis-Viva equation. Assuming instantaneous impulses, the change in velocity is simply the difference between the velocity of the elliptical orbit at r_1 to r_2 and the velocity of the circular orbit with radius r_1. Therefore:

$$\Delta V_1 = \sqrt{GM\left(\frac{2}{r_1} - \frac{2}{r_1 + r_2}\right)} - \sqrt{GM\left(\frac{1}{r_1}\right)} \tag{52}$$

Where the left hand term is the velocity of an elliptical orbit from r_1 to r_2 at r_1 and the right hand term is the velocity on the circular orbit with radius r_1.

By taking a factor of $\sqrt{\frac{GM}{r_2}}$ out and simplifying we get:

$$\Delta V_1 = \sqrt{\frac{GM}{r_1}}\left(\sqrt{\frac{2\left(r_1 + r_2\right)}{r_1 + r_2} - \frac{2r_1}{r_1 + r_2}} - 1\right) \tag{53}$$

$$\Delta V_1 = \sqrt{\frac{GM}{r_1}}\left(\sqrt{\frac{2r_2}{r_1 + r_2}} - 1\right) \tag{54}$$

$$\Delta V_1 = \sqrt{\frac{GM}{r_1}}\left(\sqrt{\frac{r_2}{a}} - 1\right) \tag{55}$$

For the secondary burn, the terms are reversed because the velocity of the circular orbit is larger than the velocity of an elliptical orbit at r_2 i.e. $v_{circular} - v_{elliptical}$. Therefore:

$$\Delta V_2 = \sqrt{GM\left(\frac{1}{r_2}\right)} - \sqrt{GM\left(\frac{2}{r_2} - \frac{2}{r_1 + r_2}\right)} \tag{56}$$

Where the left hand term is the velocity on the circular orbit with radius r_2 and the right hand term is the velocity of an elliptical orbit from r_1 to r_2 at r_2.

By taking a factor of $\sqrt{\frac{GM}{r_1}}$ out and simplifying we get:

$$\Delta V_2 = \sqrt{\frac{GM}{r_2}}\left(1 - \sqrt{\frac{2\left(r_1 + r_2\right)}{r_1 + r_2} - \frac{2r_2}{r_1 + r_2}}\right) \tag{57}$$

$$\Delta V_2 = \sqrt{\frac{GM}{r_2}}\left(1 - \sqrt{\frac{2r_1}{r_1 + r_2}}\right) \tag{58}$$

$$\Delta V_2 = \sqrt{\frac{GM}{r_2}}\left(1 - \sqrt{\frac{r_1}{a}}\right) \tag{59}$$

C.3 Launch Alignment

Starting from Keplar's third law I can derive the required launch alignment between the two celestial bodies:

$$\frac{P^2}{a^3} = \frac{4\pi^2}{GM} \tag{60}$$

Where P is the orbital period, a is the semimajor axis, G is the gravitational constant and M is the mass of the Sun.
Rearranging:

$$P^2 = \frac{4\pi^2 a^3}{GM} \tag{61}$$

$$P = 2\pi\sqrt{\frac{a^3}{GM}} \tag{62}$$

On a Hohmann transfer, the time taken from the inner to outer body is half an elliptical orbit, therefore:

$$t = \frac{P}{2} \tag{63}$$

Subbing in:

$$t = \pi\sqrt{\frac{a^3}{GM}} \tag{64}$$

using the definition for the semimajor axis $a = \frac{r_1+r_2}{2}$:

$$t = \pi\sqrt{\frac{(r_1+r_2)^3}{8GM}} \tag{65}$$

Using the angular velocity, ω of the outer body:

$$\omega_2 = \sqrt{\frac{GM}{r_2^3}} \tag{66}$$

The launch alignment can be defined as:

$$\alpha = \pi - \omega t \tag{67}$$

Subbing in:

$$\pi - \pi\sqrt{\frac{GM}{r_2^3}}\sqrt{\frac{(r_1+r_2)^3}{8GM}} \tag{68}$$

Simplifying:

$$\alpha = \pi\left(1 - \sqrt{\frac{(r_1+r_2)^3}{8r_2^3}}\right) \tag{69}$$

$$\alpha = \pi\left(1 - \frac{1}{2\sqrt{2}}\sqrt{\left(\frac{r_1}{r_2}+1\right)^3}\right) \tag{70}$$